



Formation evaluation and reservoir quality assessment of the Albian clastic sequence in the SWM Oilfield, Southwest the Mesopotamian Basin, Iraq

Riadh Ashoor¹ · Bassem S. Nabawy² · Adel Kamel¹

Received: 14 March 2022 / Accepted: 22 August 2022 / Published online: 7 September 2022
© The Author(s) 2022, corrected publication 2022

Abstract

This work intends to delineate the petrophysical properties and the reservoir quality of the Albian sequence in the Mesopotamian Basin which has been deposited as a siliciclastic sequence. The well log data (including the caliper, gamma-ray, density, photoelectric factor 'PEF', neutron, sonic, and resistivity logs), derived from eight wells in the SWM (Southwest Mesopotamian) Oilfield, was studied and interpreted using the appropriate software (IP3.6). These borehole data indicate the necessity to divide the sequence into five reservoir rock units (U1, U2, M, L1, and L2 units). This enabled depicting the porosity, shale volume, water saturation, and net-pay thickness in the vertical and horizontal directions. It is indicated that the M and L1 units are the most promising units with good to very good porosity ($\phi \geq 17.2\%$), low water saturation ($S_w \leq 28.0\%$), and acceptable shale volume ($V_{sh} \leq 8.4\%$). The net-pay thickness varies between 32.8 and 77.4 m in the different wells of the SWM Oilfield. The well log data were supported by more detailed conventional core data including porosity (ϕ_{He}) and permeability (k), from which the reservoir quality parameters were estimated precisely. In the present study, reservoir quality assessment based on conventional core data is considered for the first time for evaluating and discriminating the Albian–Aptian sequence in the Southwest Mesopotamian field into reservoir zones and hydraulic flow units. The estimated reservoir parameters include the Flow Zone Indicator (FZI), the Reservoir Quality Index (RQI), and the effective pore radius (R_{35}). Based on the available core data and the estimated reservoir quality parameters, the studied sequence was divided into three reservoir rock types (RRT1–3). The best petrophysical properties have been assigned for the medium-grained sandstone of the RRT1 that dominates in the L1 and the M units (av. $\phi_{He} = 23.0\%$, av. $k = 1581$ mD, av. $R_{35} = 23.7$ μm , av. $FZI = 7.368$ μm , and av. $RQI = 2.304$ μm). On the other side, the fine-grained sandstone of the RRT3 is characterized by the lowest petrophysical properties and reservoir quality parameters (av. $\phi_{He} = 17.1\%$, av. $k = 5.49$ mD, av. $R_{35} = 0.92$ μm , av. $FZI = 0.603$ μm , and av. $RQI = 0.136$ μm). The integration between the well log and core data of the studied Albian sequence stated that the M and L1 units are the most promising reservoir units. They are predominated by medium-grained and fine to medium-grained sandstones of the RRT1 and the RRT2, respectively. This well log-core data integration is applicable to the different oilfields in the different fields in the Mesopotamian Basin and other basins in south Iraq and elsewhere.

Keywords Mesopotamian basin · Well log · Core data · Reservoir quality · Petrophysical assessment · Rock typing · Clastic sequence · South Iraq

✉ Bassem S. Nabawy
bsnabawy@yahoo.co.uk; bs.nabawy@nrc.sci.eg

Riadh Ashoor
mmmjd89@yahoo.com

Adel Kamel
adelkamel@mans.edu.eg

¹ Geology Department, Faculty of Science, Mansoura University, Mansoura, Egypt

² Department of Geophysical Sciences, National Research Centre, Giza, Egypt

List of symbols

A	Cross-sectional area, cm^2
a	Lithology exponent, 0.0
ΔP	Pressure difference, N/m^2
ΔT_{\log}	Sonic velocity from log, $\mu\text{s/ft}$
Δt_f	Sonic fluid velocity, $\mu\text{s/ft}$
Δt_{ma}	Sonic matrix velocity, $\mu\text{s/ft}$
ϕ_D	Density porosity, 0.0
ϕ_e	Effective porosity, 0.0
ϕ_{He}	Helium porosity, %
ϕ_N	Neutron porosity, 0.0

\emptyset_T	Total porosity, 0.0
FR	Formation resistivity factor, 0.0
FZI	Flow zone indicator, μm
GR	Gamma-ray, API
k	Permeability, millidarcy mD
L	Plug length, cm
μ	Viscosity, centipoise cp
m	Porosity exponent, 0.0
n	Saturation exponent, 0.0
Q	Flow rate, cm^3/s
R_{35}	Is the effective pore radius, μm^2
ρ_{Log}	Density value from log, g/cc
ρ_f	Density of fluid, g/cc
ρ_{ma}	Density of matrix, g/cc
Ish	Shale index, 0.0
V_{clay}	Clay volume, 0.0
VSH	Shale volume, 0.0

Abbreviations

DRT	Discrete rock type
IP	Interactive petrophysics
LLD	Deep latero log resistivity, ohmm
LLS	Shallow latero log resistivity; ohmm
NPI	Normalized Porosity Index, 0.0
NPHI	Neutron log, 0.0
PEF	Photoelectric factor, b/e
RHOB	Density log, g/cc
RQI	Reservoir quality index, μm
RRT	Reservoir rock type
Rw	Water resistivity, ohmm
RT	True resistivity, ohmm
SP	Spontaneous potential log, mV
SW	Water saturation, 0.0
SWM	Southwest Mesopotamian
V_b	Bulk volume, cc
V_g	Grain volume, cc

Introduction

The Mesopotamian Basin is among the most promising hydrocarbon basins in south Iraq. It covers a vast area of the central parts of Iraqi lands and extends to the south; it extends in the area between the Euphrates and the Tigris rivers (Fig. 1). Geology and lithostratigraphy of the Mesopotamian basin were studied by many authors. It is situated on the unstable shelf of the Arabian Peninsula and is composed of a complex pattern of river channels, alluvial fans, deltas, flood plains, marshes, and sabkha (Buday and Jassim 1984, 1987; Numan 2000; Fouad 2010; Handhal et al. 2019).

It produces hydrocarbons from many oil and gas fields. Among these, the SWM (Southwest Mesopotamian) Oilfield in the southwest of the Mesopotamian Basin constitutes

an oil-bearing structure of conformed several reservoirs. It produced oil from the first exploratory well by the Iraqi Oil Company in 1948. The SWM Oilfield has located 70 km from Basra city and 12 km from the Rumaila Oilfield (Alhakeem et al. 2019). It produces from multi-reservoirs with the main production obtained from the Albian sequence. It has been firstly discovered by Glynn Jones in 1948 at the Nahr Umr Oilfield with thicknesses reaching up to 360 and 400 m in south Iraq and Kuwait (Bellen et al. 1959; Khudhair and Al-Zaidy 2018). Its thickness in the SWM Field attains 200–240 m. In its type section in southern Iraq, the Albian sequence comprises black shales interbedded with medium to fine-grained sandstone with some lignite, amber, and pyrite content (Bellen et al. 1959).

In the SWM Field, the Albian sequence is considered among its most prolific sequences. It is unconformably underlain by the Shuaiba Formation. It is a siliciclastic sequence with a few limestone and dolostone interbeds. It is dominated by a varicolored, fine to medium-grained sand composition with a few organic materials-rich shale streaks that are dominated in the upper and middle parts of the studied sequence. The shale intercalations act as a source and sealing rocks for the oil accumulations in the lower parts of the sequence. This Albian sequence is subdivided into three main units. The lower unit (L) is further subdivided into two subunits (L1, and L2 units). The lower subunit L2 primarily consists of shales, while the subunit L1 consists of thick sandstone beds intercalated with a few shale streaks that vary in thickness from well to well as disappear in others. The middle unit (M) consists of sand and shale interbeds. Upward, the upper unit is further subdivided into two subunits (U1 and U2). The subunit (U2) is composed of non-clastic carbonate rocks, while the subunit (U1) consists of sand and shale intercalations.

The structural regime of the SWM field is simple with no dominant faults affecting its compartments (JOGEMEC 2010). Among more 50 wells were drilled in the SWM Oilfield, and only 19 wells penetrated the Albian sequence. So, due to its oil prospectivity, the reservoir characterization of the Albian clastics in the SWM Oilfield is the main target of this study.

To achieve this target, the available well log data of eight wells that penetrated the Albian sequence, were studied to define its lithology and petrophysical parameters including the net-pay thickness, porosity, shale volume, and hydrocarbon saturation.

Geologic setting

During the last decades, the lithostratigraphy and the structural setting of the Mesopotamian Basin were studied by many authors (e.g., Qaradaghi 2001; Qaradaghi et al.

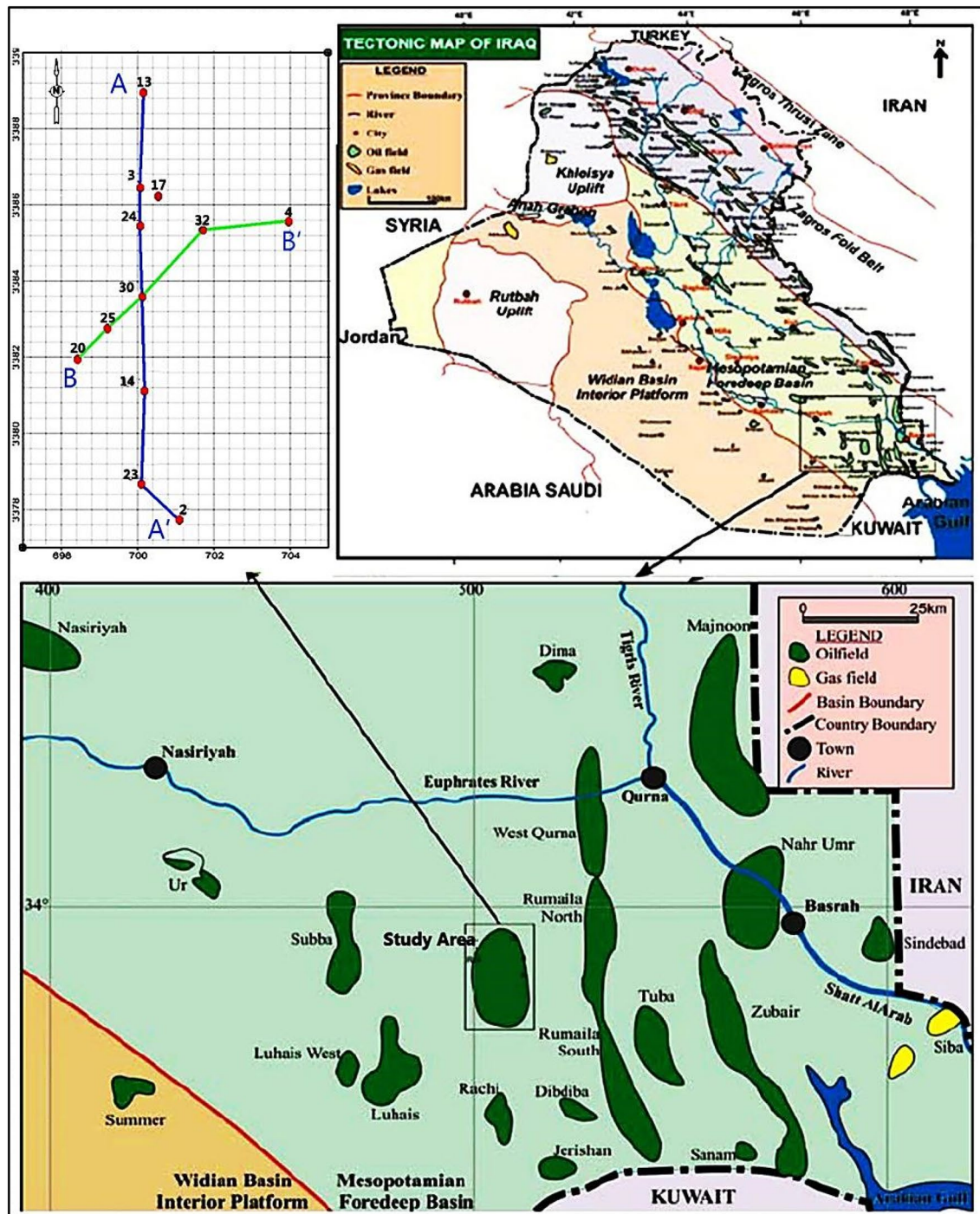


Fig. 1 Location map of the studied SWM Oil Field indicating **a** main oil fields in south Iraq, **b** the tectonic map of Iraq, and **c** the location map of the studied wells in the Albian sequence and the studied A–A' and B–B' profiles

2008; Sissakian et al. 2020). It extends between the Tigris and the Euphrates in Iraq and Syria; therefore, it almost covers most of the Iraq lands and many parts of Syria and south-eastern Turkey. It is further discriminated into northern and southern Mesopotamian basins (Wilkinson

2000; Foster and Foster 2009; Canard 2011; Sissakian et al. 2020). The northern basin covers the area from Tigris in the north to Baghdad, while the southern basin extends from Baghdad to the Arabian Gulf in the south (Foster and Foster 2009; Canard 2011).

Lithostratigraphy

The Albian sequence was firstly described by Owen and Nasr (1958) at its type section at NU-2 well in the Nahr Umr Oilfield in the southern province of Iraq lands. Its stratigraphy and geologic setting were studied and described in detail by many authors (Bellen et al. 1959; Buday 1980; Jassim et al. 1984; Qaradaghi 2001; Qaradaghi et al. 2008; Khudhair and Al-Zaidy 2018). An Albian age is suggested for this sequence and applied for the present work.

It is primarily composed of friable to medium-hard, and fine to coarse-grained varicolored cross-bedded sandstone intercalated with dark to reddish cross-laminated brown shale interbeds. These shales are occasionally fissile with some pyrite and lignite content and rich in organic matter. It is locally encountered in the studied wells and regionally in the different parts of the Mesopotamian Basin with a variable thickness. In the west and southwest of the basin, it is a siliciclastic sequence dominated by sand content, while it is dominated by shale interbeds to the east of the basin (Jassim and Goff 2006; Qaradaghi 2001; Qaradaghi et al. 2008). Some non-clastic limestone and dolostone interbeds are encountered in the section s intercalations with siltstone and shale beds throughout the different levels of the section.

The Albian sequence is overlain conformably by the regionally extended Mauddud Formation, sometimes with a gradational contact. Its upper contact is assigned between the basal dolostone and limestone beds of the Mauddud Formation and the uppermost sandstone and shale beds of the Albian sequence. Also, it is unconformably underlain by the Shuaiba Formation. This unconformable contact is assigned between the yellow to pale grey dolostones of the Shuaiba Formation and the basal dark fissile shales of the Albian sequence (Fig. 2) (Qaradaghi 2001; Qaradaghi et al. 2008).

Structural outlines

The study area is located in the Stable Arabian Shelf tectonic regime. The alignment of most fields in the study area along the N–S direction is due to the interplay of the Pre-Cambrian N–S aligned basement faults and the Infra-Cambrian salt-associated tectonics (Alhakeem et al. 2019). The Albian–Aptian rifting is formed due to the tension forces between the Bitlis/Sirjan and the northern borders of the Arabian plate (Arfania and Shahriari 2009).

The Albian–Aptian structure features were mostly inherited from the Jurassic Gotnia Basin and were activated during the Berriasian time. This indicated that the tectonic history of the Arabian plate was governed by all tectonic movements that happened along its margins due to the Mesozoic–Cenozoic rifting and collision between the Gondwanaland and Asia (Audley-Charles et al. 1988; Powell et al.

1988; Sadooni 1993, 1997). The main structural elements of the Mesopotamian Basin are shown in Fig. 3.

Methods and available data

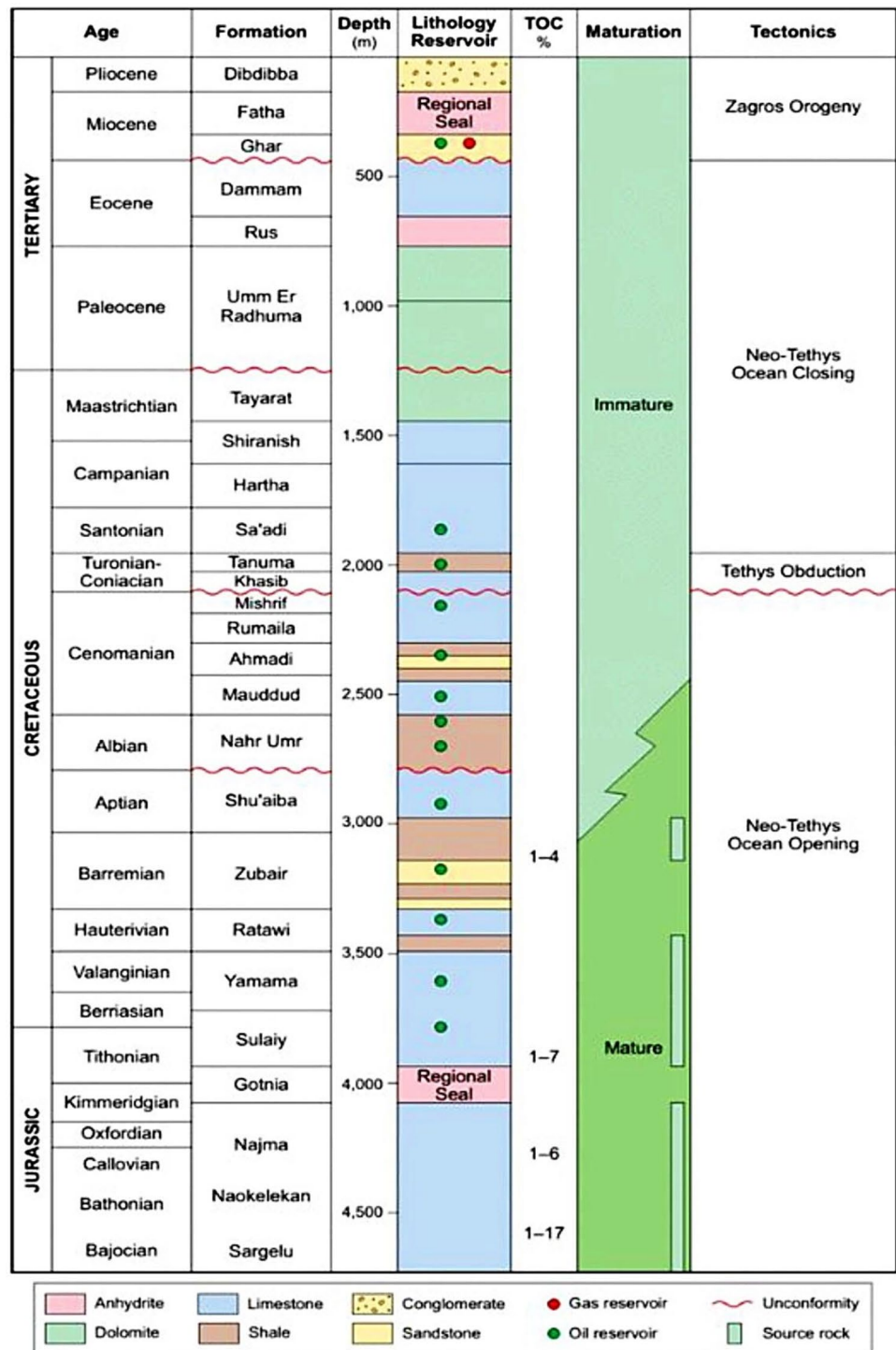
The petrophysical analysis of a given sequence is the base of the hydrocarbon-bearing reservoir potential evaluation (Shehata et al. 2021; Nabawy et al. 2022; Haque et al. 2022; Fallah-Bagtash et al. 2022; Kassem et al. 2022). This includes lithologic interpretation from the X–Y cross-plots of some petrophysical parameters, the net-pay zones and their parameters from the litho-saturation vertical plot, and the contour maps of the petrophysical parameters in the different wells (Baouche and Nabawy 2021; Abdeen et al. 2021; Kassem et al. 2022).

In this concern, the hydrocarbon prospectivity of the clastic Albian sequence in the SWM Oilfield has been evaluated using the available well log data of 8 wells (A-4, A-14, A-17, A-20, A-23, A-25, A-30, and A-32, Fig. 1). The LAS files format of these borehole logs was processed and studied using the Senergy IP3.6 following a systematic workflow procedure as shown in Fig. 4. The type of the drilling fluid, the borehole temperature, and the borehole properties were considered during the processing and interpretation of the petrophysical data (Nabawy and Shehata 2015; Abuamarah et al. 2019; Radwan et al. 2021; Abdelwahhab et al. 2022; Shehata and Sarhan 2022). Before processing the well log data, it was required to correct the available data to the environmental conditions. This was achieved using the Schlumberger charts (Schlumberger 1984, 1991, 1995) to rectify logs and modify them to the standard condition using the IP3.6 software.

Available data

The available logging data of the Albian sequence include the gamma-ray (GR), bulk density (RHOB), neutron porosity (NPHI), sonic (ΔT), and the shallow and deep resistivity logs (LLS, LLD, respectively). Also, the temperature log, the mud filtrate resistivity, and the mud resistivity values were all available and applied for correcting the resistivity logs. The gamma-ray curve was used for discriminating the reservoir zones from the non-reservoir units, while the neutron-density logs were used to identify the main reservoir units (El Sharawy and Nabawy 2018). In addition to the litho-saturation plots, lithology was investigated in all wells using a set of logging cross-plots including the density-neutron and the gamma-ray-neutron cross-plots. Increasing the shale content shifts the data points away from the pure sand baseline due to the presence of secondary porosity and/or gas content (Schlumberger 1984, 1991, 1995).

Fig. 2 A generalized lithostratigraphic column of the Mesopotamian Basin in south Iraq (Al-Ameri et al. 2009)



Lithology estimation

To estimate lithology types, different methods were applied using the IP software V3.6, such as density-neutron, neutron-sonic, and M–N mineralogy identification cross-plots, where Eqs. (1) and (2) can be used to estimate the M and N

values (Radwan and Nabawy 2022). The matrix identification (MID) involves estimating the apparent matrix density (Δm_a) and the apparent transit time of rock matrix (Δt_{ma}) as in Eqs. (3 and 4).

$$M = (\Delta T_f - \Delta T_{log}) / (\rho_{Log} - \rho_f) \times 0.01 \tag{1}$$

Fig. 3 A Schematic sketch showing the main structural elements crossing through the SWM Oil Field at SWM-A-3 well, the Mesopotamian Basin, Iraq

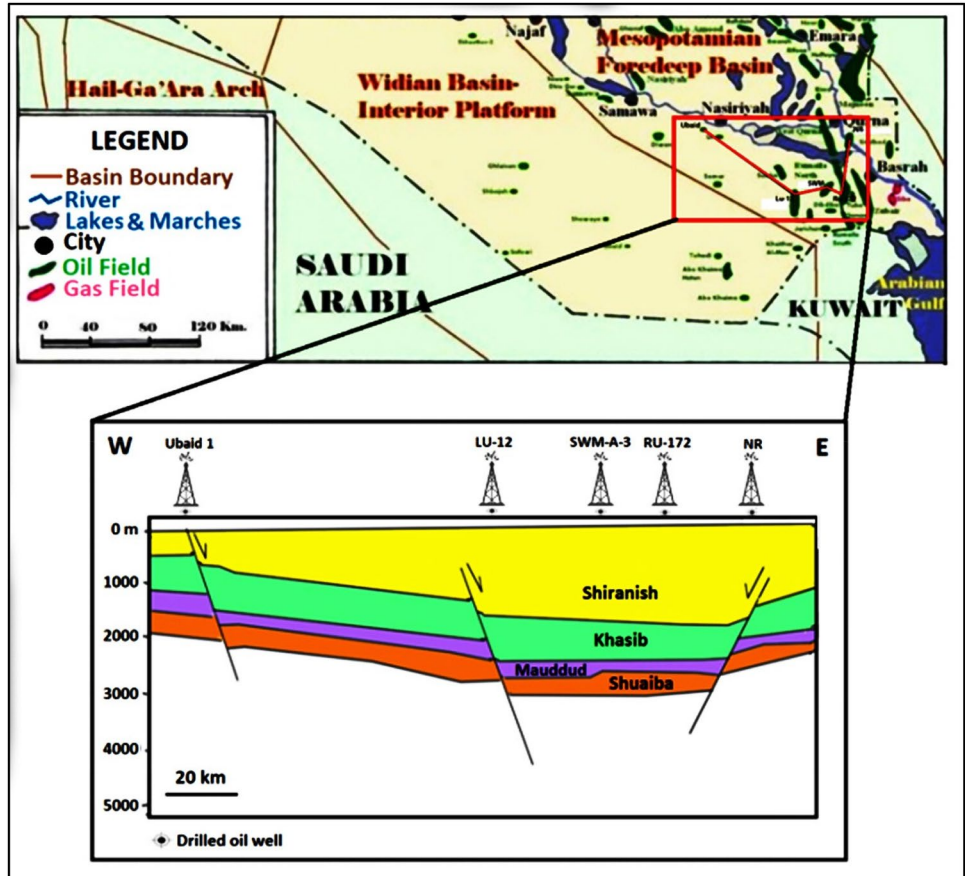
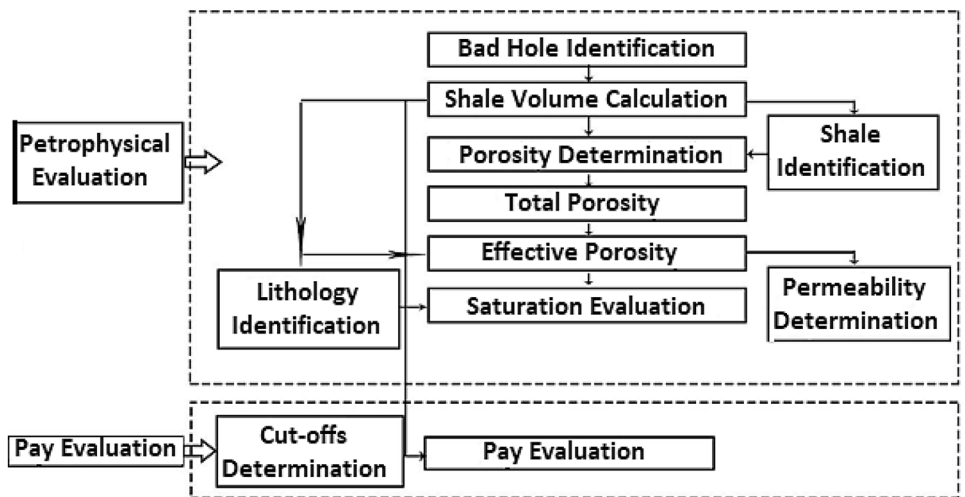


Fig. 4 The applied workflow procedure processing and interpreting the petrophysical data and the pay evaluation of the Albian sequence in SWM Oil Field



$$N = (1 - \phi_{Log}) / (\rho_{Log} - \rho_f) \tag{2}$$

$$\Delta T_{ma} = (\Delta T_{log} - \Delta T_f \cdot \phi_T) / (1 - \phi_T) \tag{3}$$

$$\rho_{ma} = (\rho_b - \phi_T \cdot \rho_f) / (1 - \phi_T) \tag{4}$$

where ρ_f is the fluid density, ρ_{Log} is the density log reading, ΔT_{Log} is the transit time log reading, ΔT_f is the transit time for fluid, ϕ_{Log} is the porosity log reading, ΔT_{ma} is the transit time for matrix, ϕ_T is the total porosity, and ρ_{ma} is the matrix density.

Shale volume estimation

The shale volume (V_{sh}) is among the governing parameters of the reservoir rocks, where its increase causes a decrease in the effective porosity and permeability of the reservoir rocks. Also, the conductive clay minerals reduce the formation resistivity factor (FR), so the shaly sand reservoirs need a specific petrophysical workflow to estimate the implementation of the bound water on their petrophysical properties and quality (David et al. 2015; Elgendy et al. 2020). To perform the well log data corrections and the shale volume correction, the impact of the bound water should be considered to estimate the effective porosity and hydrocarbon saturation (Heslop and Heslop 2003; Ezz El-Din et al. 2013; Teama and Nabawy 2016). For the present study, the shale volume of

the Albian sequence in the studied wells was estimated using single and double indicators following six procedures including gamma-ray, spontaneous potential (SP), density-neutron, sonic-neutron, and sonic-density. Based on these procedures, it is indicated that the gamma-ray log reveals the most actual value (Fig. 5). Then, the shale volume was corrected using the following equation (Larionov's 1969).

$$V_{sh} = 0.083 \times (2^{3.7 \times Ish} - 1) \tag{5}$$

where Ish is the gamma-ray index value that can be estimated as follows (Asquith and Gibson 1982).

$$Ish = (GR_{Log} - GR_{min}) / (GR_{max} - GR_{min}) \tag{6}$$

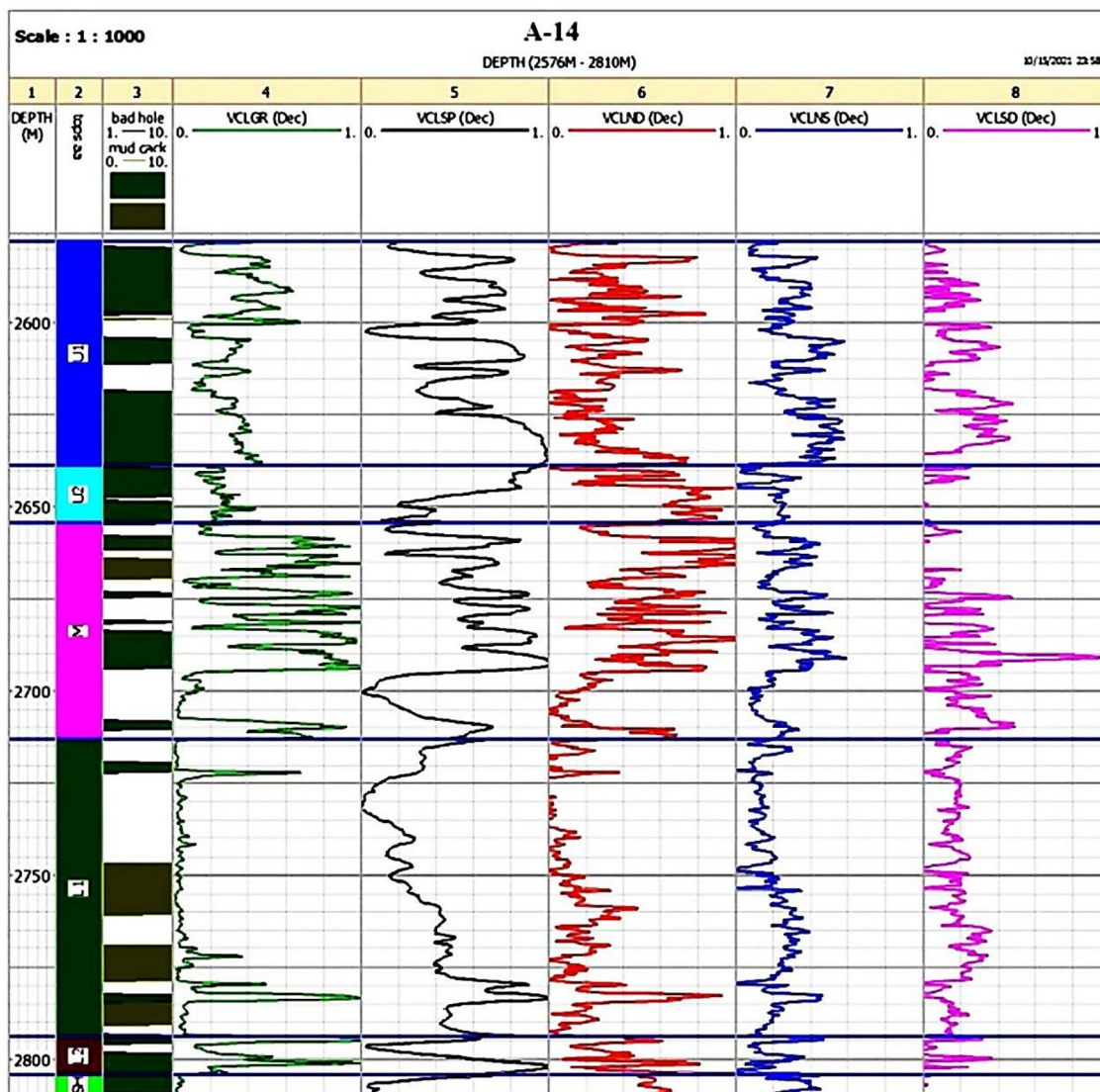


Fig. 5 Determining the shale volume of the Albian sequence in A-14 well using different techniques

Porosity estimation

The total porosity value (\emptyset_T) was estimated using the density-neutron porosity model of Asquith (1982) (Schlumberger 1984).

$$\emptyset_T = (\emptyset_N + \emptyset_D)/2 \quad (7)$$

where \emptyset_T is the total porosity, \emptyset_D is the density porosity, and \emptyset_N is the neutron porosity.

The density porosity can be estimated as follows (Schlumberger 1984).

$$\emptyset_D = (\rho_{ma} - \rho_b)/(\rho_{ma} - \rho_f) \quad (8)$$

where ρ_{ma} is the matrix density, ρ_b is the bulk density log reading, and ρ_f is the matrix density.

The effective porosity was then calculated after correcting the total porosity value by removing the pores contributed due to the shale content (Schlumberger 1984).

$$\emptyset_e = \emptyset_T(1 - V_{clay}) \quad (9)$$

Water saturation (Sw)

Many equations have been introduced to determine the water saturation. Archie's equation is the most common equation that can be applied for clean sandstone reservoirs. Archie's Eq. (1942) can be applied to calculate the water saturation in the un-invaded clean reservoir zones where the shale content is less than 10% (Archie 1942).

$$S_w^n = FR.Rw/R_T = a.Rw/R_T.\emptyset^m \quad (10)$$

where FR is the formation resistivity factor, Rw is the formation water resistivity, RT is the true resistivity values measured in the un-invaded zone, a is the lithology factor, and m is the porosity exponent. The Archie's parameters including the lithology factor (a), the porosity exponent (m), and the saturation exponent (n) are required to assess the water saturation of the studied reservoir, i.e., its hydrocarbon content to differentiate between the potential and non-potential oil-bearing zones. The Picket plot is the most common technique that can be utilized to achieve this target. It is based on plotting the deep resistivity as a function of porosity at different points and assuming $a = 1$, $n = 2$, then the m value can be determined as the slope of the obtained line by knowing the Rw values (Fig. 6) (El Sharawy and Nabawy 2018). For the Albian sequence, the porosity exponent fluctuates between 1.72 and 2.0.

Besides, there are many equations like Simandoux and the Indonesian equations that can be applied to the argillaceous sandstone reservoirs ($V_{sh} > 10\%$), where the water

saturation was determined using the Simandoux equation (Asquith and Krygowski 2004) (Simandoux 1963).

$$S_w = (a.Rw)/(2.\emptyset^m). \{SQRT[(V_{sh}/R_{sh})^2 + ((4 * \emptyset^m)/(a.Rw.R_T))] - (V_{sh}/R_{sh})\} \quad (11)$$

For the present study, we have applied Archie's equation for the clean reservoir zones, while the applied Simandoux equation was applied for the argillaceous zones.

Net-pay thickness determination

To divide the reservoir sequence into zones potential and non-potential zones and to define the net-pay thickness, a porosity cutoff equal to 10%, water saturation of 40%, and a shale volume equal to 40% were applied. Thereby, the net-pay thickness was estimated based on considering all intervals in which the effective porosity values exceed 10%, and their water saturation and shale volume values are less than 40%. The reservoir properties and the static model of the Albian reservoir are discussed in the following sections and tabulated in Table 1.

Measured core data

A total of 148 plug samples, representatively cored from the Albian sequence, were drilled out of the cored intervals of three wells (A-02, A-14, and A-17 wells) in SWM Oilfield. They are selected representatively for the different sedimentary facies. Then porosity and permeability of these samples were measured. The bulk volume (v_b , in cm^3) and weight of the plugged samples were measured after drying for two days at 60 °C. The grain volume (v_g , in cm^3) was then measured by a helium pycnometer (14.5 psi) and the helium porosity (\emptyset_{He}) was estimated as follows.

$$\emptyset_{He} = 100 \times (v_b - v_g)/v_b \quad (12)$$

Permeability (k) of the plug samples was measured in mD using a nitrogen permeameter using the following equation.

$$k = (Q \times \mu \times L)/(DP \times A) \quad (13)$$

where Q = flow rate in cm^3/s , μ = air viscosity in centipoise, L = plug length in cm, A = cross-sectional area in cm^2 , and ΔP = the differential pressure in atm/cm.

The reservoir quality concept was applied to evaluate the reservoir quality, where the flow zone indicator (FZI in μm), the reservoir quality index (RQI in μm), and the normalized porosity index (NPI in decimals) were calculated using porosity (\emptyset , in decimals) and permeability (k, in md) as follows.

$$NPI = \emptyset/(1 - \emptyset) \quad (14)$$

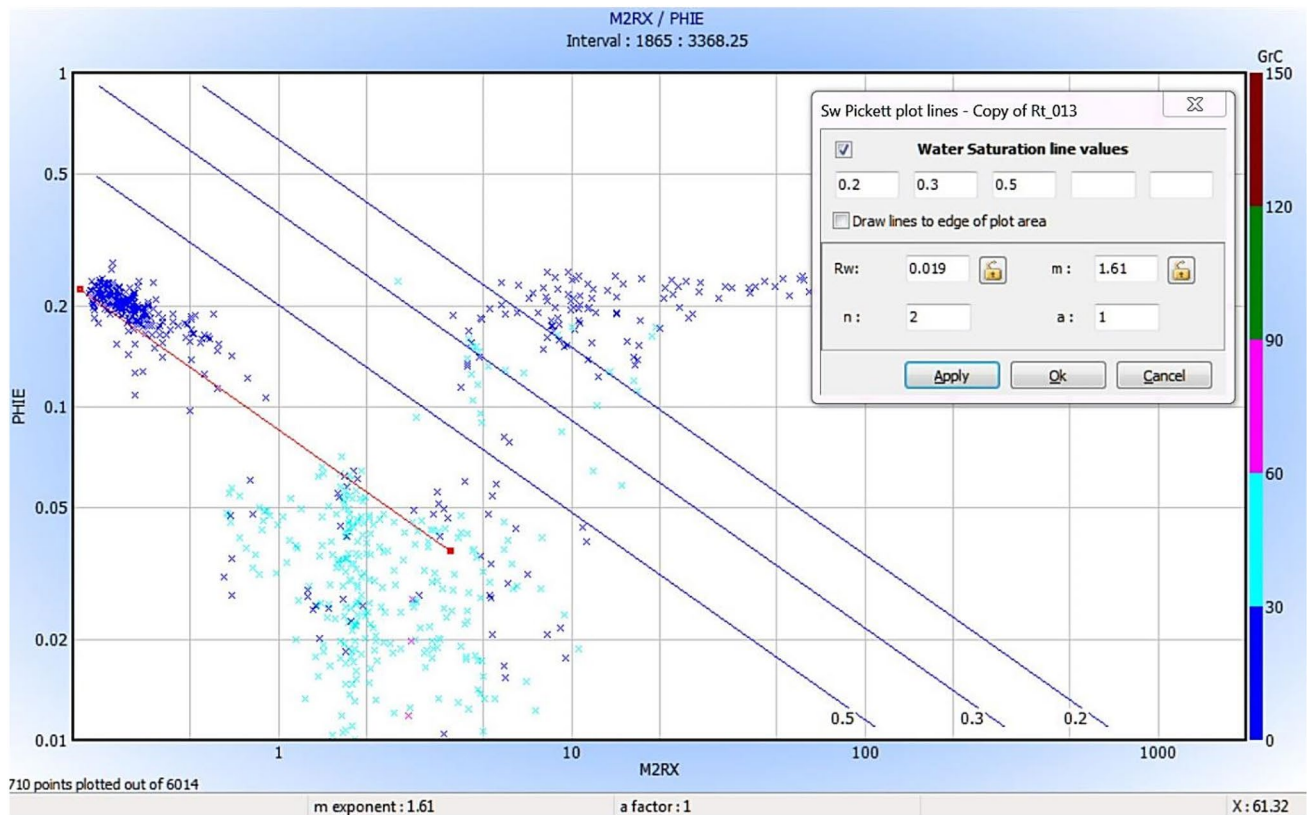


Fig. 6 Pickett plot for estimating the porosity exponent value (m) by knowing the formation water resistivity value (R_w), A-13 well. GR is the gamma-ray values

$$RQI = 0.0314 \times \text{SQRT}(k/\phi) \quad (15)$$

$$FZI = RQI/NPI \quad (16)$$

Amaefule et al. (1993).

Rock typing was performed using the porosity–permeability plot supported by the discrete rock type values (DRT, Shenawi et al. 2007) which can be estimated using the following model (Nabawy and El Sharawy 2018).

$$DRT = \text{Round}(2 \times \text{Ln}(FZI) + 10.6; 1) \quad (17)$$

The average effective pore throat radius (R_{35} , in μm) of Winland (1972) is considered a measuring reservoir quality parameter, so it was estimated for each plug sample using the following model (Winland 1972).

$$\text{Log}(R_{35}) = 0.732 + 0.588 \log(k) - 0.864 \log(\phi_{He}) \quad (18)$$

More details on the applied measuring techniques are described in many publications (e.g., Nabawy 2013; Nabawy et al. 2015, 2020a, b, c; Elgendy et al. 2020; El Sawy et al. 2020; Abuamarah and Nabawy 2021; Shehata et al. 2021; Abdelmaksoud and Radwan 2022; Radwan

and Nabawy 2022; etc.) The measured core data of the different petrophysical rock types are tabulated in Table 2.

Results

Petrophysical evaluation

For the Albian sequence in the SWM Oilfield, a gross thickness was estimated as 191.6–243.0 m in the different wells (Table 1). Based on the estimated shale volume and resistivity values along this gross thickness, the Albian reservoir has been subdivided into five reservoir zones (Fig. 5); from top to bottom it is U1 (2577.5–2639 m), U2 (2639–2654 m), M (2654–2713.5 m), L1 (2713.5–2794 m), and L2 (2794–2804 m) units. A sixth shaley zone (SH) was added at depth interval 2804–2810 m which was excluded from the gross thickness. From this zonation, it is indicated that the lower shale volume is assigned to the L1 unit, while the higher one was assigned to both U1 and L2 (Fig. 5). The petrophysical properties of the estimated gross thickness, in particular, the shale volume and porosity percentage vary from level to level in the studied wells in SWM

Table 1 The petrophysical parameters, based on the borehole data, of the Albian reservoir in the SWM Oil Field

Well No	Top (m)	Bottom (m)	Gross thickness (m)	Net-pay (H) (m)	N/G	Phi _e	S _w	S _o	V _{sh}	Phi*H	Phi*So*H
A-02	2613.9	3023.0	220.1	40.4	0.184	0.201	0.194	0.816	0.072	8.12	6.63
A-14	2577.7	2810.0	226.3	67.6	0.291	0.220	0.113	0.897	0.034	14.87	13.34
A-17	2581.5	2827.0	243.0	73.3	0.302	0.198	0.070	0.93	0.011	14.51	13.50
A-20	2607.1	2824.0	191.6	41.3	0.216	0.199	0.241	0.769	0.023	8.22	6.32
A-23	2595.8	2801.4	205.6	61.9	0.301	0.191	0.281	0.729	0.032	11.82	8.62
A-25	2589.6	2812.7	223.1	76.5	0.343	0.192	0.264	0.746	0.084	14.69	10.96
A-30	2576.5	2791.4	214.9	77.4	0.360	0.199	0.121	0.889	0.049	15.40	13.69
A-32	2592.1	2821.3	229.1	32.8	0.143	0.172	0.196	0.814	0.029	5.64	4.59

N/G is the net-pay to gross ratio, Phi_e is the average effective porosity, S_w is the average water saturation, S_o is the average oil saturation, and V_{sh} is the average shale volume

Oilfield (Fig. 7a, b). The average shale volume (V_{sh}) varies between 1.1 and 8.4% indicating the predominance of clean sandstone (V_{sh} < 10%), while the effective porosity was estimated to vary between 17.2 and 22.0% for the different wells (Table 1). The water saturation of the Albian reservoir is less than 30% (7.2–28.1%), while the oil saturation varies between 72.3 and 92.9% (Table 1), i.e., it is a highly potential reservoir. These prospective petrophysical values resulted in a good Phi*H and Phi*So*H vary from 5.64 to 15.4 and from 4.59 to 13.69, respectively.

The litho-saturation plot of the A-14 well (Fig. 7a) states that the U1, U2, and M units have the highest GR value (track 1) and shale volume (track 8). Increasing the shale volume of these units caused some washing out in these units as indicated from the caliper in track 1 (Fig. 7a, b). A cross-over is indicated between the density and neutron logs in track 6 for A-14 and A17 wells (Fig. 7a, b) which is well developed, particularly through the L1 unit and the lower part of the M unit. Thereby, the L1 and M units represent the main prospective reservoir units in the Albian sequence. Also, plotting the water saturation, the movable and non-movable hydrocarbon saturations in track 7, for both A-14 and A-17 wells, states the presence of good amounts of movable hydrocarbon in the lower parts of the M unit and the upper parts of the L1 unit extending for about 57 m depth interval in A-14 well (2700–2757 m, Fig. 7a), and 83 m depth interval in A-17 well (2673–2756 m, Fig. 7b).

Net-pay thickness

Plotting the effective porosity as a function of the shale volume for the A-14 well (as an example for the studied wells) indicates that most of the assigned reservoir readings are characterized by gamma-ray values less than 37.5 API and sometimes up to 75 API. This is probably due to a relatively high feldspathic content (Fig. 8a). Besides, plotting the water saturation as a function of the effective porosity indicates that most readings have GR values less than 60 API (Fig. 8b). So to estimate the net-pay thickness of the Albian reservoir sequence, a porosity cutoff value was applied as 10%, while the applied cutoff values for the shale volume and the water saturation were 40% (Fig. 8a, b).

Also, to define the net-pay thickness, it is needed to define accurately the water–oil contact (OWC) in the different wells based on the deep resistivity values. The vertical plotting of the water saturation of the Albian reservoir zones indicates that the OWC surface has been determined at depth interval 2760–2765 m for the different wells (Fig. 9). The OWC is assigned within the L1 unit; therefore, the lower parts of the L1 unit and the full thickness of the L2 unit are fully saturated with water and should not be considered during estimating the net-pay thickness. The upper parts of the L1 unit are considered oil-bearing zones, while many streaks of

Table 2 Porosity, permeability, and reservoir quality parameters of the cored Albian intervals in the SWM Oil Field

RRTs	<i>N</i>		DRT	\varnothing_{He}	<i>k</i>	R_{35}	NPI	RQI	FZI
			0.0	%	md	μm	0.0	μm	μm
RRT1	106	Min	13.0	9.2	15.4	3.95	0.101	0.406	3.368
		Max	15.5	30.6	4800	43.4	0.441	4.047	11.70
		Avg	14.5	23.0	1581	23.7	0.303	2.304	7.368
RRT2	30	Min	10.5	6.00	0.23	0.48	0.06	0.061	0.961
		Max	12.9	30.1	488	10.8	0.43	1.264	3.220
		Avg	11.8	19.2	97.0	4.37	0.25	0.525	1.940
RRT3	12	Min	8.0	12.0	0.16	0.22	0.136	0.036	0.268
		Max	10.5	26.2	25.3	2.15	0.355	0.309	0.952
		Avg	9.4	17.1	5.49	0.92	0.211	0.136	0.603

where *N* is the number of samples; DRT is the discrete rock type values; \varnothing_{He} is the effective porosity; *k* is the nitrogen permeability; R_{35} is the effective pore radius of Winland (1972); NPI is the normalized porosity index; RQI and FZI are the reservoir quality and the flow zone indicator, respectively

the overlying middle unit (M), the lower parts of the upper unit (U1), and the full sequence of U2 are fully saturated with water ($S_w = 100\%$, Fig. 9). This may indicate two or more compartments which are partially isolated within the Albian reservoir. Therefore, the total net-pay thickness was estimated as 32.8–77.4 m in the different wells (Table 1).

Lithology determination

To determine the lithology of the Albian reservoir units, the litho-saturation plot (Fig. 7a, b) was applied in addition to a set of cross sections/profiles including the density-neutron, M–N, and density-sonic cross-plots (Fig. 10a, b, c). The gamma-ray readings in the litho-saturation plot indicate that the high intensity of shale streaks is assigned to the U2, in particular at its lower part (2645–2654 m, Fig. 7, tracks 2, 6), which is mostly composed of argillaceous limestone. Plotting the density as a function of the neutron indicates that most points are slightly affected by the shale and the calcareous content of the studied samples (30–60 API, Fig. 10a). The implication of the shale and calcareous content causes scattering and shifting of most samples toward higher density (limestone and dolomite lines) and porosity value ($0.15 \leq \text{NPHI} \leq 0.60$, Fig. 10a). Besides, estimating the M and N values and plotting them on the M–N cross-plot for each rock unit indicates that readings of the L1 unit of the Albian sequence are shifted toward high *M* and *N* values which may be attributed to the presence of some salts and/or hydrocarbons content with relatively high porosity values (Fig. 10b). The measured points of the U1 unit and the upper parts of the M unit are shifted toward relatively low *M* and *N* values due to their shaly content which is primarily calcareous as indicated from the cuttings description. On the other side, the lithology of the U2 unit is typically limestone despite shifting some readings away from the typical

argillaceous limestone composition due to its argillaceous content.

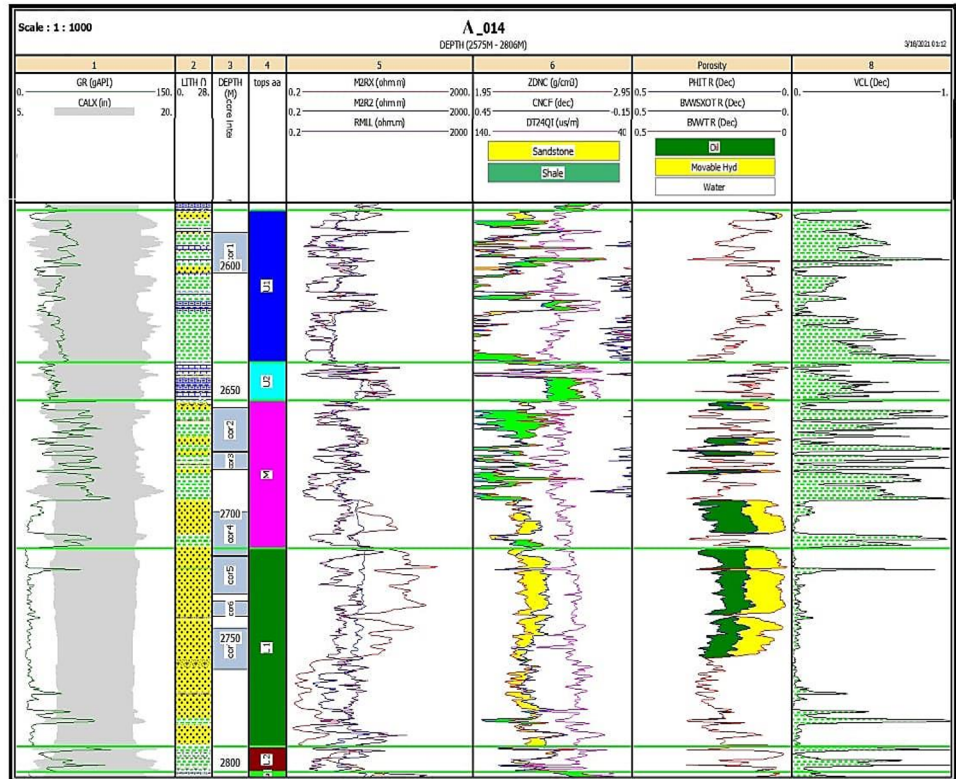
The matrix density-transit time indicates the calcareous sandstone composition of the L1 readings, where they are located on the quartz-calcite line, while readings of the other units are shifted toward higher matrix density values due to their shale content (Fig. 10c).

Iso-parametric maps for the petrophysical properties

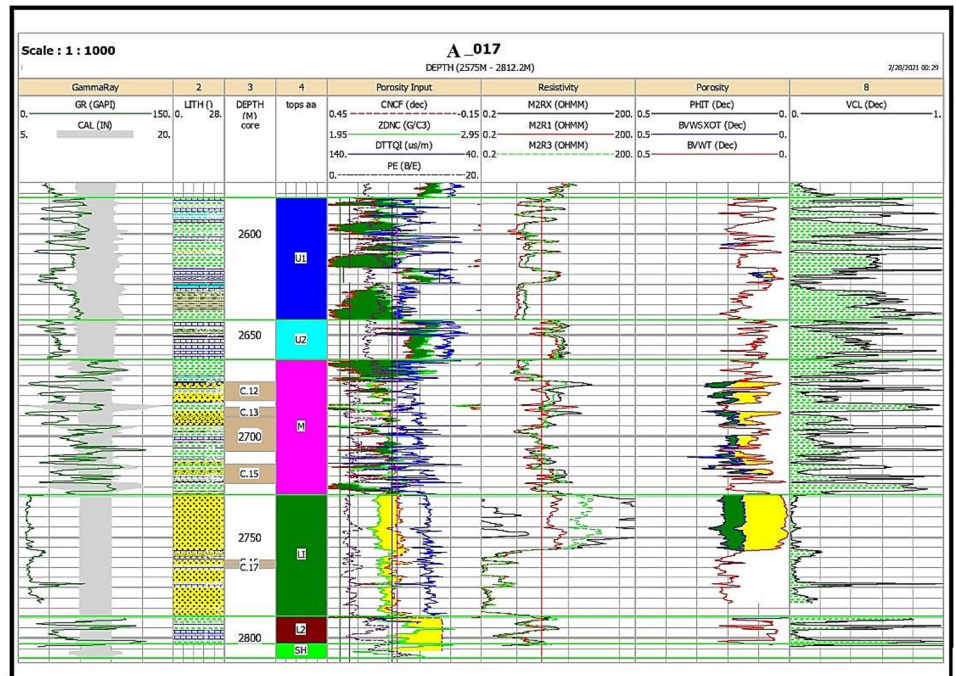
To check the lateral variation of the petrophysical properties, and the net-pay thickness, a set of iso-parametric maps were constructed to follow up on these parameters through the SWM Oilfield to help in designing future exploration and development plans. Plotting the water and oil saturations for the studied wells as contour maps indicates that the lower water saturation and in turn the higher hydrocarbon content is assigned for A-14, A-17, and A-30 wells (Table 1). Plotting the water and oil saturations as iso-parametric maps indicates decreasing the water saturation (S_w) toward the central parts at the A-14 well and to the north at the A-17 well (Fig. 11a) which shows the lowest water saturation at the A-14 and A-17 wells (Fig. 11b). The highest water saturation and the lowest oil saturation are assigned at A-25 and A-23 wells in a saddle form (Fig. 11a, b).

To follow the lateral change in the storage capacity of the Albian sequence, the effective porosity values were presented as an iso-parametric map indicating the highest values at the A-14 well and also at the A-17 and A-30 wells but with fewer values (Fig. 11c). Values of the shale volume (V_{sh}) as an indication of the reservoir ability to deliver its oil content were presented as a 2D map showing the highest shale volume at A-25 and A-2 wells, i.e., the shale volume increases to the west and southeast of the study area (Fig. 11d).

Fig. 7 Litho-saturation vertical plot indicating the different petrophysical values for the Albian sequence reservoir zones in A-014 well (a) and A-017 well (b)



(a)

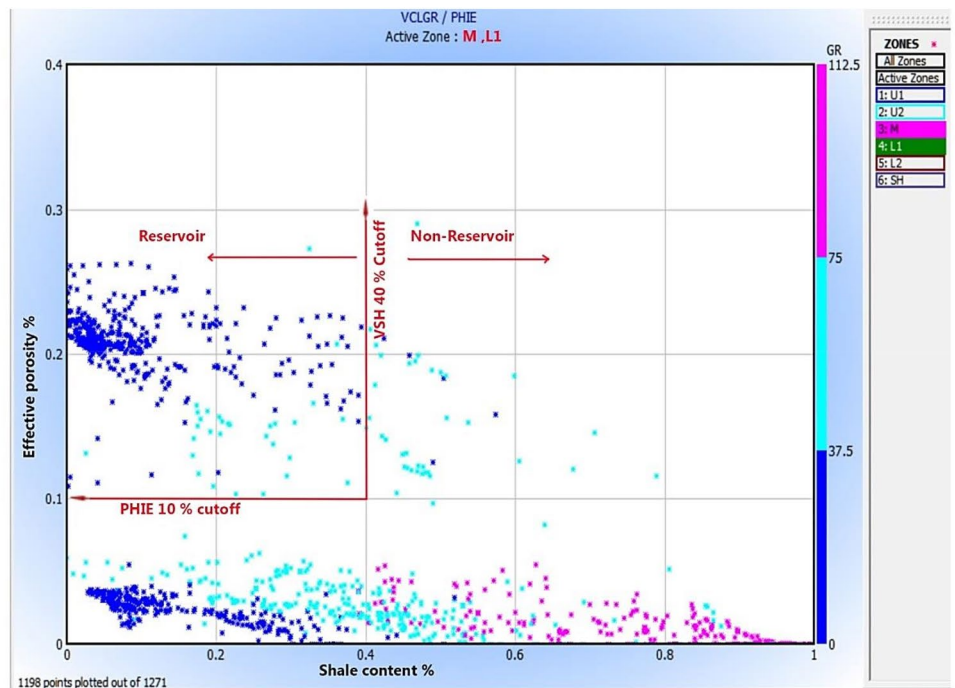


(b)

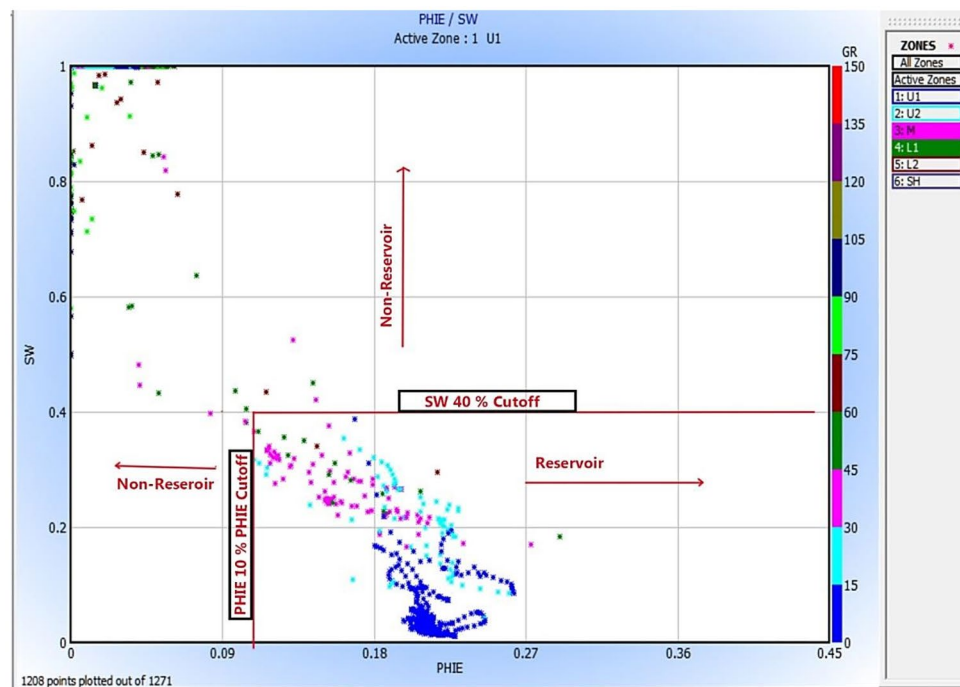
Considering the aforementioned iso-parametric maps and the cutoff values (10% for porosity, and 40% for both the water saturation and the shale volume), it is indicated that the best net-pay thickness was estimated in the northeast

direction at the A-17 and in the central parts at the A-14, A-17, A-25, and A-30 wells (Fig. 12). The relatively high net-pay thickness of the studied reservoir sequence at A-25 well to the west is accompanied by a prospective

Fig. 8 Discriminating the reservoir and non-reservoir intervals in A-14 well using **a** the shale content-effective porosity cross-plot and **b** the effective porosity (Phie)-water saturation (Sw) cross-plot for A-14 well. The colored bar to the right indicates the gamma-ray values (GR)



(a)



(b)

range of reservoir parameters ($S_w = 26.0\%$, $V_{sh} = 8.4\%$, and $\phi_e = 19.2\%$, Fig. 12, Table 1). The deterioration of the petrophysical properties to the west of the SWM Field may be attributed to increasing the implementation of the

diagenetic processes which caused a slight increase in the shale volume and the water saturation due to increasing the complexity of pore throat distribution, i.e., increasing the retained water content.

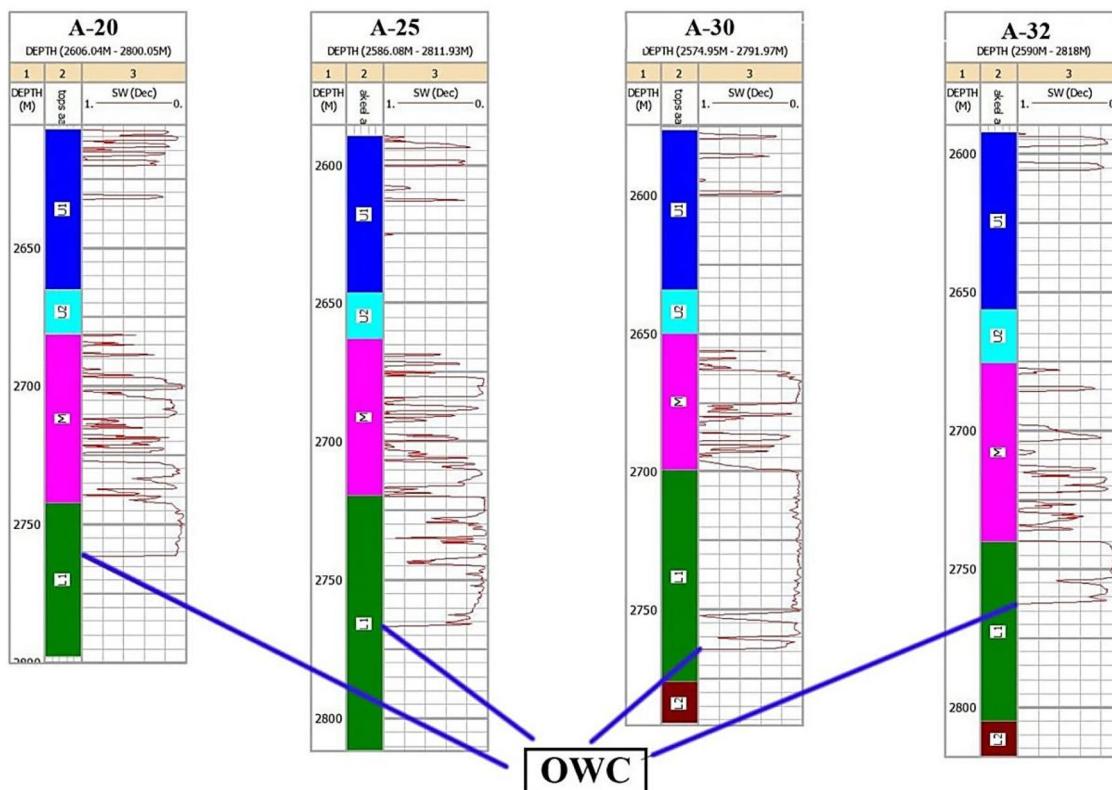


Fig. 9 The oil–water contact (OWC) determination based on estimating the water saturation (SW) based on the deep resistivity values, the SWM Oil Field

Lateral distribution

To follow up on the lateral variation of the Albian thickness in the SWM Oilfield, the GR and lithology were correlated through two profiles crossing the field in the N–S and the NE–SW directions (Fig. 13 a, b). Based on these profiles, it is indicated that the thickness of the Albian sequence increases in the central parts of the SWM Field and its N–S direction reaching 409.1 m at the A-02 well and 245.5 m at the A-17 well. Also, it is stated that the lower parts of the upper unit (U2), which is composed of limestone, show consistency in thickness distribution through the different parts of the field. On the other side, the L1 unit is dominantly composed of sandstone with a few shale streaks and is well represented in A-14, A-25, A-30, and A-32 wells in the middle parts of the field (Fig. 13a), while its thickness is slightly reduced to the west at A-20 well (Fig. 13b).

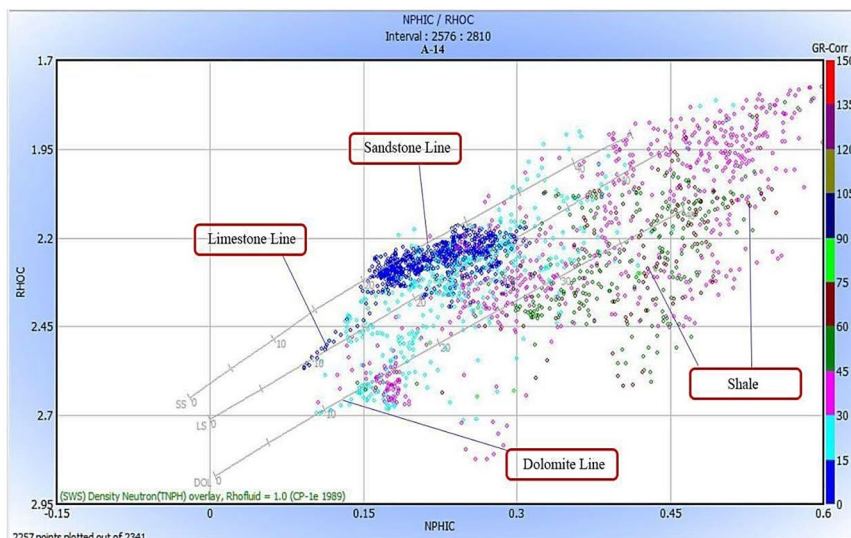
Following up the structural setting and depth interval for the different wells indicates a doubly plunging anticline oriented along the north–south direction with a slight change in thicknesses of the different reservoir units (Fig. 14).

Conventional core data

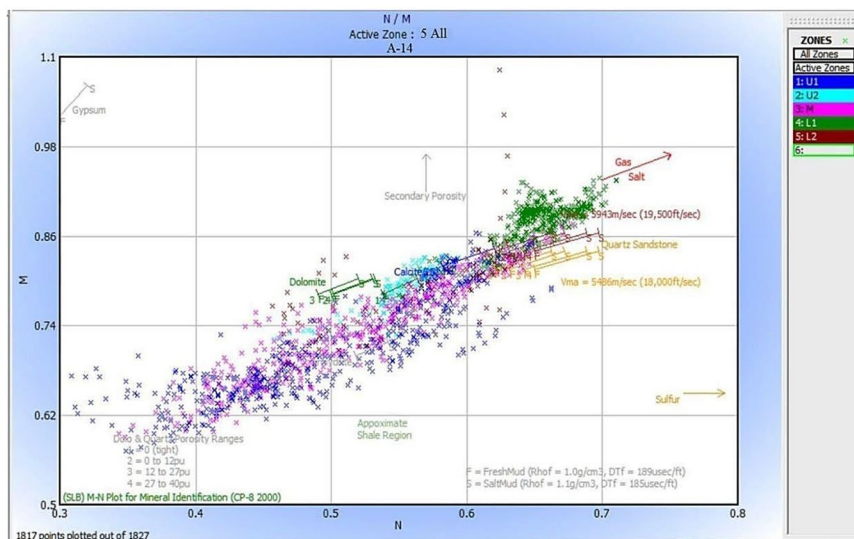
Reservoir rock typing

In SWM Oilfield, the studied samples were discriminated into three reservoir rock types (RRTs) considering that the porosity contribution to permeability for all samples of the same rock type is equal. Among these, the RRT1 samples (71.6% of the studied samples) are representative of the top parts of the L1 unit, and the upper and lower parts of the M unit of the Albian sequence, whereas the RRT2 and RRT3 samples (28.4%) are intercalated with each other representing the main body of the M unit. Plotting the permeability as a function of porosity is presented by a best-fit line of each rock type with high reliability ($R^2 > 0.80$, Fig. 15). Dividing the samples into rock types using this plot should be done based on the discrete rock type values (DRT) of the different samples (Radwan et al. 2022a, b). The higher the porosity contribution to the permeability is always accompanied by higher DRT values and higher reservoir quality, where the DRT values of the RRT1 samples that have the best reservoir quality vary from 13.0 to 15.5, whereas for the RRT3 samples that have the lowest reservoir quality, the DRT values are located

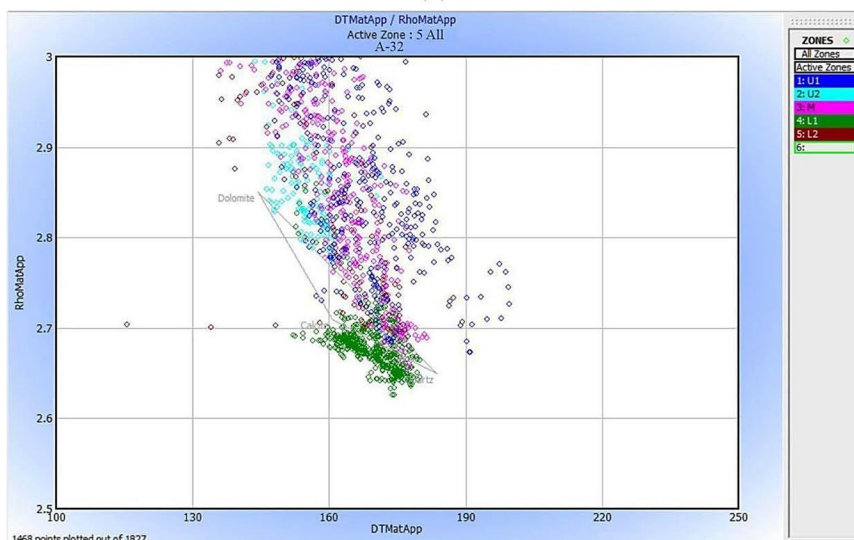
Fig. 10 Lithology determination of the Albian sequence in A-17 well using **a** the density (RHOC)-neutron porosity (NPHIC) cross-plot, accompanied with the gamma-ray bar (GR), **b** M–N cross-plot, and **c** matrix density (RHOMat)-transit time (DT) cross-plot



(a)

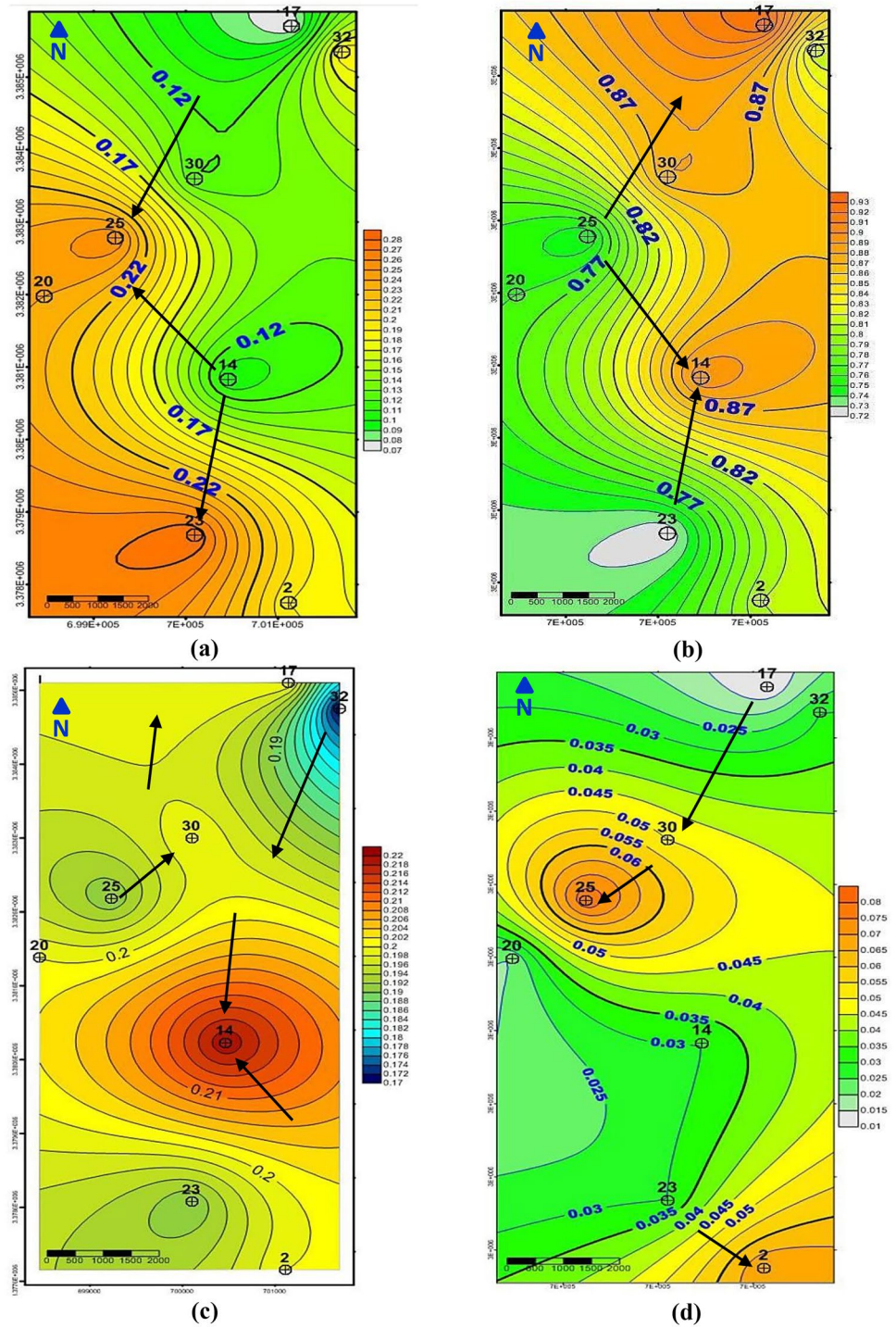


(b)



(c)

Fig. 11 Iso-parametric maps for the studied Albian sequence showing **a** the water saturation (S_w in 0.0), **b** oil saturation (S_o in 0.0), **c** effective porosity (ϕ_e in 0.0), and **d** the shale volume (V_{sh} in 0.0). Arrows refer to the direction of increasing values



in between 8.0 and 10.5. The RRT2 group is considered a transitional group between these RRTs. It is indicated that the porosity and permeability of almost samples are higher than the porosity cutoff (10%) and the permeability cutoff value (1.0 mD). Based on this plot and the present study, the permeability can be estimated using the following mathematical model.

$$RRT1 : k = 1 \times 10^{-4} \phi_{He}^{5.09} \quad (R^2 = 0.825) \quad (19)$$

$$RRT2 : k = 2 \times 10^{-5} \phi_{He}^{4.94} \quad (R^2 = 0.873)$$

$$RRT3 : k = 9 \times 10^{-7} \phi_{He}^{5.30} \quad (R^2 = 0.808)$$

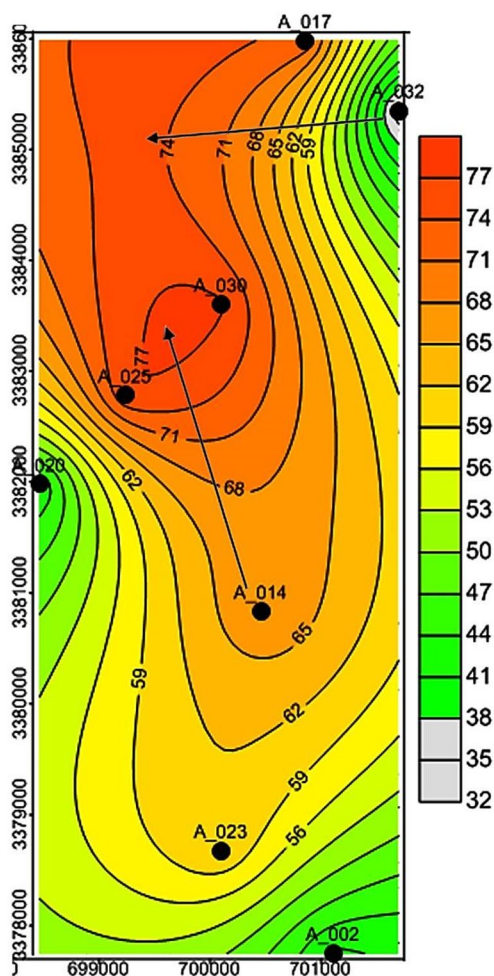


Fig. 12 Iso-parametric map representing the net-pay thickness (in feet) of the Albian sequence in the SWM Oil Field. Arrows refer to the direction of increasing thickness

Discussion

In this section, the implementation of the different petrophysical parameters on each other and their mutual relationships will be established and interpreted.

Permeability (*k*) dependence on the pore throat size (*R*₃₅)

The dependence of the permeability on the pore throat connections is higher than its dependence on the pore volume; i.e., it is not only directly proportional to the porosity but also the effective pore radius *R*₃₅ of Winland (1972) as stated in literature (Liu et al. 2019; Lai et al. 2019, 2020; Abuhagaza et al. 2021; Safa et al. 2021; Shehata et al. 2021). Therefore, plotting the permeability as a function of both porosity and *R*₃₅ (Fig. 16) indicates that the good to excellent permeability values of the RRT1 samples are due to the predominance of

the macropore sizes (*R*₃₅ > 5.0 μm). On contrary, the poor to fair permeability values of the RRT3 samples are due to the dominance of meso- to micropore sizes (0.22 < *R*₃₅ < 2.15 μm, Fig. 16, Table 2). The transitional RRT2 samples are primarily represented by mesopore spaces.

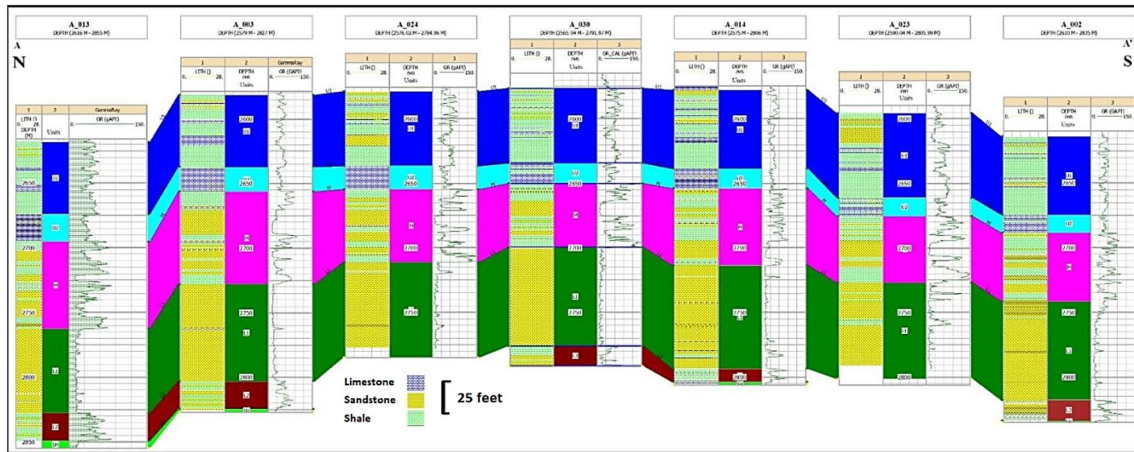
The macropore sizes of the RRT1 samples are attributed to their clastic composition and sedimentary structures as described from the cutting samples, where they consist of thick medium-grained sandstones intercalated with a few shale streaks. On the other side, the RRT2 and RRT3 samples, which represent the middle most parts of the M unit, are composed of fine to medium-grained sandstone with frequent shale streaks.

The reservoir quality attributes

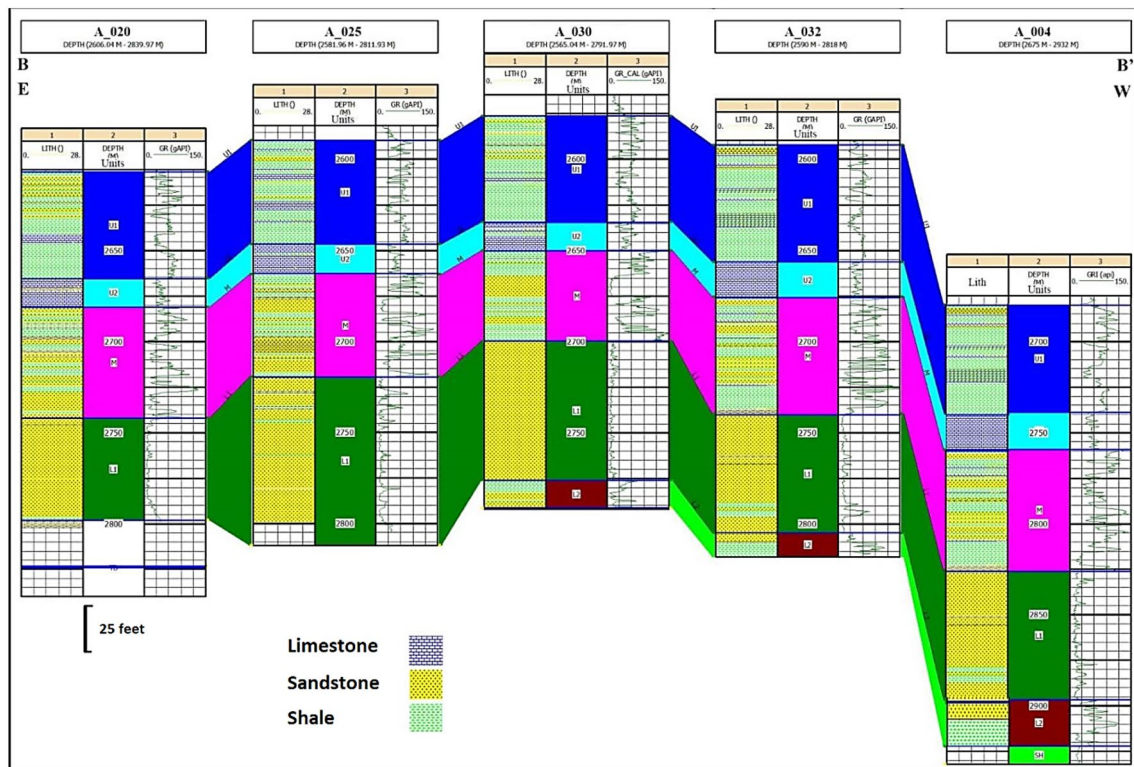
The reservoir quality index (RQI) is a direct measure of the ratio between the flow and the storage capacities of the given reservoir rock which is in turn dependent on both porosity and permeability (Nabawy et al. 2018a, b). So, plotting the RQI as a function of permeability indicates that the RQI is exponentially related to the permeability as a measure of the reservoir flow capacity for the different rock types (*R*² ≥ 0.989, Fig. 17a). The RQI of the RRT1 samples is primarily characterized by fair to very good quality (0.406 ≤ RQI ≤ 4.047 μm of average RQI = 2.304 μm, Fig. 17a, Table 2), whereas the RRT2 samples are characterized by fair average reservoir quality (av. RQI = 0.525 μm, Fig. 17a, Table 2). The variation in the reservoir quality of the RRT1 and RRT2 samples may be attributed to the differential implementation of the reducing and enhancing diagenetic factors that affected the reservoir quality.

As aforementioned, in addition to the dependence of the RQI on permeability, plotting the RQI as a function of porosity indicates also its subsidiary dependence on porosity as a measure of the reservoir storage capacity (0.820 ≥ *R*² ≥ 0.733, Fig. 17b). Scattering the data on the porosity-RQI plot may be attributed to the complexity of the spatial pore fabric and due to its main contribution to the permeability (Fig. 17a, b). This explanation is supported by the fact that the studied RRTs of the Albian samples are characterized by the same porosity range (fair to excellent, 6.0–30.6%, Fig. 17b, Table 2). The RQI of the Albian samples can be estimated using the following mathematical models.

$$\begin{aligned}
 RRT1 : RQI &= 0.115k^{0.42} \quad (R^2 = 0.992) \\
 RQI &= 0.0035\phi_{He}^{2.05} \quad (R^2 = 0.753) \\
 RRT2 : RQI &= 0.099k^{0.41} \quad (R^2 = 0.994) \\
 RQI &= 0.001\phi_{He}^{1.97} \quad (R^2 = 0.820) \\
 RRT3 : RQI &= 0.082k^{0.42} \quad (R^2 = 0.992) \\
 RQI &= 0.0003\phi_{He}^{2.11} \quad (R^2 = 0.733)
 \end{aligned}
 \tag{20}$$



(a)



(b)

Fig. 13 Lateral variation of the Albian reservoir units in SWM Oil Field along **a** A–A' profile trending N–S, and **b** B–B' profile trending NE–SW direction. Profiles' directions are illustrated in Fig. 1

The RQI-k model's exponents (0.41–0.42) and their multiplication factors (0.082–0.115) of the different rock types are similar to each other; therefore, the RQI of the Albian RRTs can be estimated in terms of k using a general model as follows.

$$AIRRTs : RQI = 0.088 k^{0.46} \quad (R^2 = 0.995) \quad (21)$$

Also, presenting the RQI as a function of the FZI is a widely applied procedure to evaluate the reservoir quality. Considering the classification of the reservoir ranks of Nabawy et al. (2018a, b), the RRT1 samples of the Albian sequence are characterized by fair to very good RQI values,

Fig. 14 3D-structural contour maps on top surfaces of the Albian reservoir units (U1, U2, M, and L1 units) in the SWM field

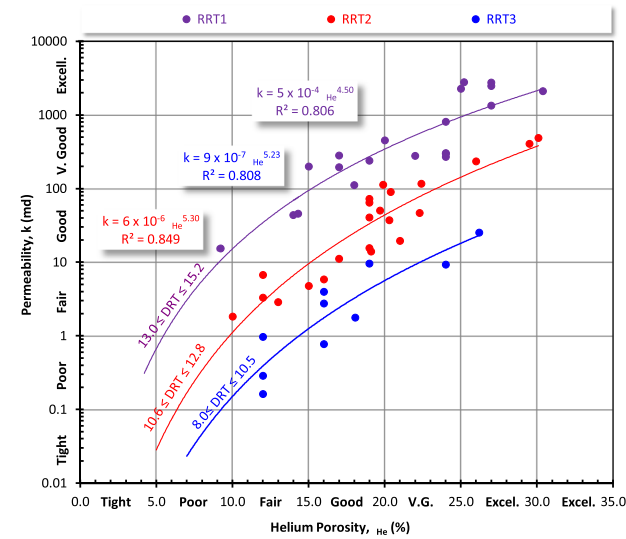
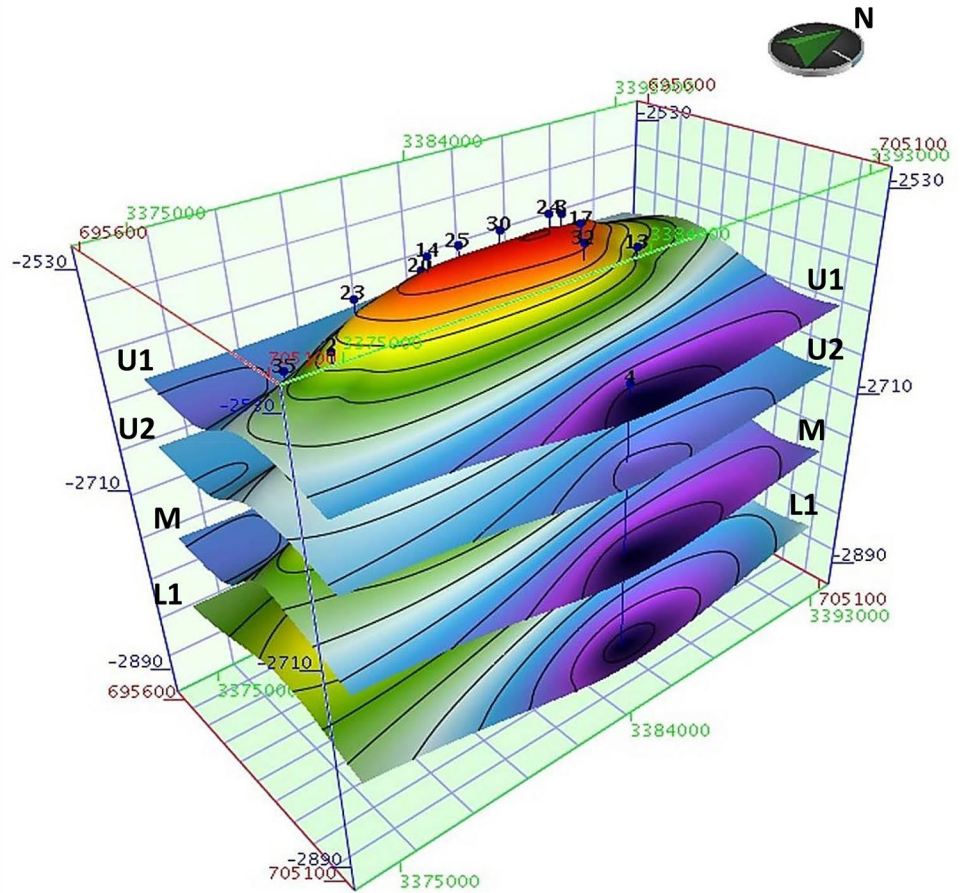


Fig. 15 Rock typing of the promising Albian sequence (M and L1 units) based on the porosity, permeability, and discrete rock type (DRT) values

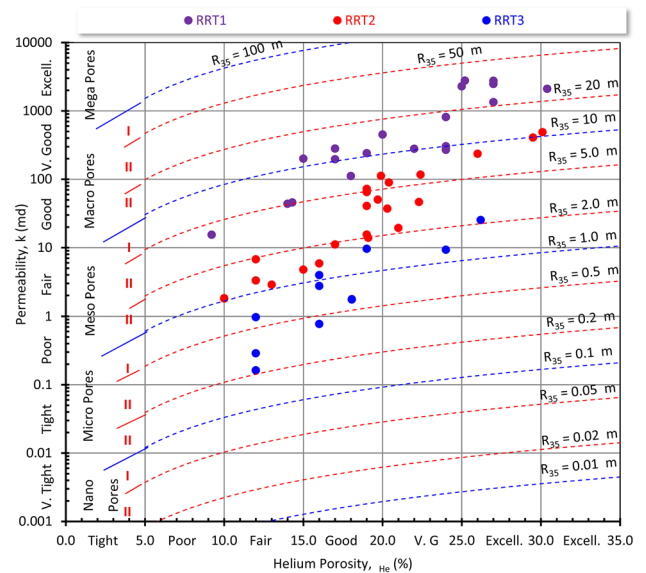
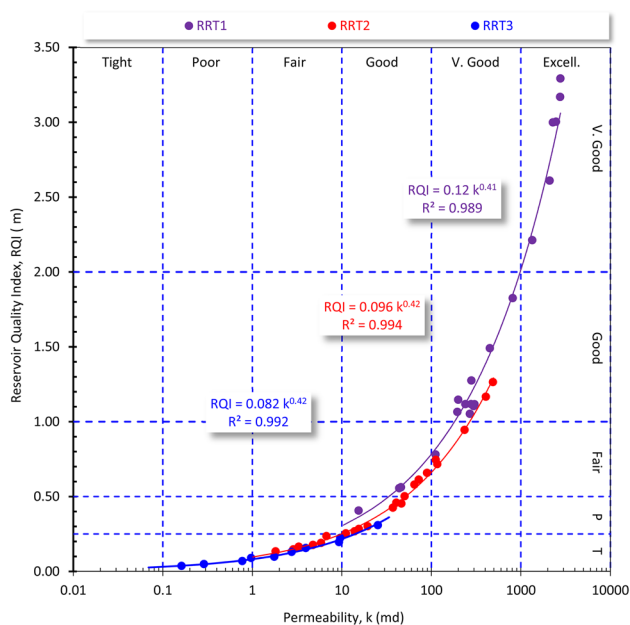
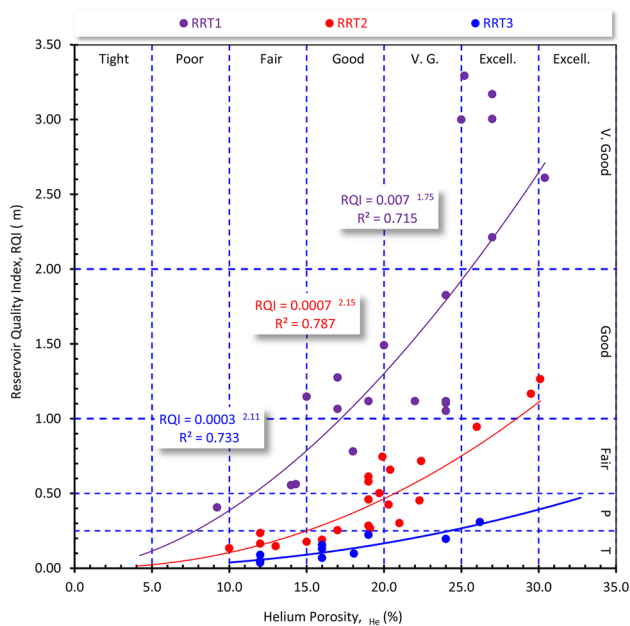


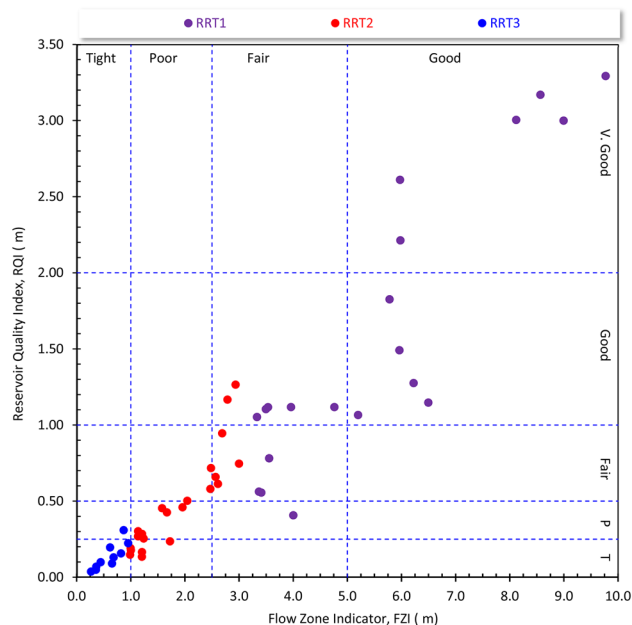
Fig. 16 Effective pore throat sizes estimated as R_{35} values of the Albian reservoir rock types in the M and L1 units



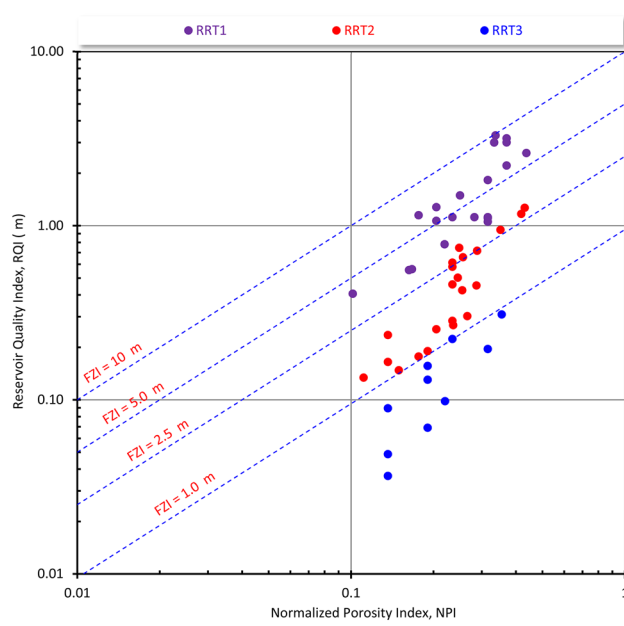
(a)



(b)



(a)



(b)

Fig. 17 Dependence of the reservoir quality index (RQI) of the core samples on **a** permeability, and **b** porosity. P and T refer to poor and tight qualities, respectively

the RRT2 samples are of tight to good reservoir quality, while the RRT3 samples are considered tight (Fig. 18a). The tightness of the RRT3 samples is also attributed to their low FZI values, whereas the RRT1 samples have fair to good FZI values. These fair to very good RQI and FZI values of the RRT1 samples and the tightness of the RRT3 are primarily attributed to their macropore spaces ($3.95 \leq R_{35} \leq 43.4 \mu\text{m}$, Fig. 16, Table 2).

Fig. 18 Presenting the reservoir quality index (RQI) versus **a** the flow zone indicator (FZI), and **b** the normalized porosity index (NPI) superimposed by the FZI values of the Albian sequence. P and T refer to poor and tight qualities, respectively

Besides, presenting the RQI versus the normalized porosity index NPI supports dividing the Albian samples into three RRTs, with the RRT3 being characterized by tight reservoir quality ($\text{FZI} \leq 0.96 \mu\text{m}$), while the RRT2 ($0.96 \leq \text{FZI} \leq 3.22 \mu\text{m}$) and the RRT1 ($3.30 \mu\text{m} \leq \text{FZI}$) samples are considered of poor and fair to good reservoir quality, respectively (Fig. 18b).

Reservoir zonation based on the vertical plot of the core data

The reservoir zonation based on the core data is a widely applied procedure to divide the reservoir sequence into some hydraulic flow units (HFUs) each with its diagnostic petrophysical values (Nabawy et al. 2022). Plotting the porosity, permeability, RQI, FZI, and the R_{35} values as functions of depth accompanied by their corresponding reservoir rock types of the top L1 unit and the lower part of the M unit indicates the dominance of the RRT1 samples through the top of the L1 unit. The L1 and the lower parts of the M units represent the HFU-3 and are composed of the RRT1 samples. They are characterized by inconsistent petrophysical behavior with two peaks of relatively high petrophysical values at 2715.5 m depth and the middle parts of the L1 unit at 2763.5 m depth (Fig. 19). The second HFU-2 extends from depth 2688.8 to 2715.5 m. Though its prospective petrophysical values, its behavior is spiky, especially in its middle parts with micro- to macropore spaces (R_{35}) with some non-prospective streaks. This can be attributed to its alternative composition of the RRT2 and the RRT3 samples with more dominance of the RRT2 samples.

Upward, the HFU-1 extends from a depth of 2675–2688.8 m and it is characterized by somewhat better petrophysical values than the underlying HFU-2. The spiky behavior of this flow unit is due to its differential

composition of the RRT1 and RRT2 samples with a few RRT3 samples. It is characterized mostly by mesopore spaces and it is considered entirely prospective (Fig. 19).

The dominance of the spiky petrophysical behavior of the studied sequence states the high heterogeneity of the Albian reservoir due to the intercalation between the fine to medium-grained sandstones and the shale beds along the entire sequence. These shale intercalations are more predominated in the M unit (HFU-1 and HFU-2) than in the HFU-3 of the L1 unit.

Regional applications for the Albian reservoirs

The Albian reservoir sequence in the Mesopotamian Basin is among the most prolific reservoirs in the Arabian Gulf from Iraq in the north to the United Arab Emirates in the south where it contains many promising reservoir and source rock units (Bellen et al. 1959; Alsharhan 1991; Al-Ameri et al. 2001; Qaradaghi et al. 2008; Al-Khafaji 2015; Khudhair and Al-Zaidy 2018; Handhal and Hussein 2020).

Consequently, studying the petrophysical properties and the reservoir characteristics of the Albian sequence using the available well log and core data in SWM Oilfield would be beneficial for a successful hydrocarbons exploration and development through the Albian sequences in their subsurface presence in south Iraq fields and their extensions along the western and eastern shorelines of the Arabian Gulf

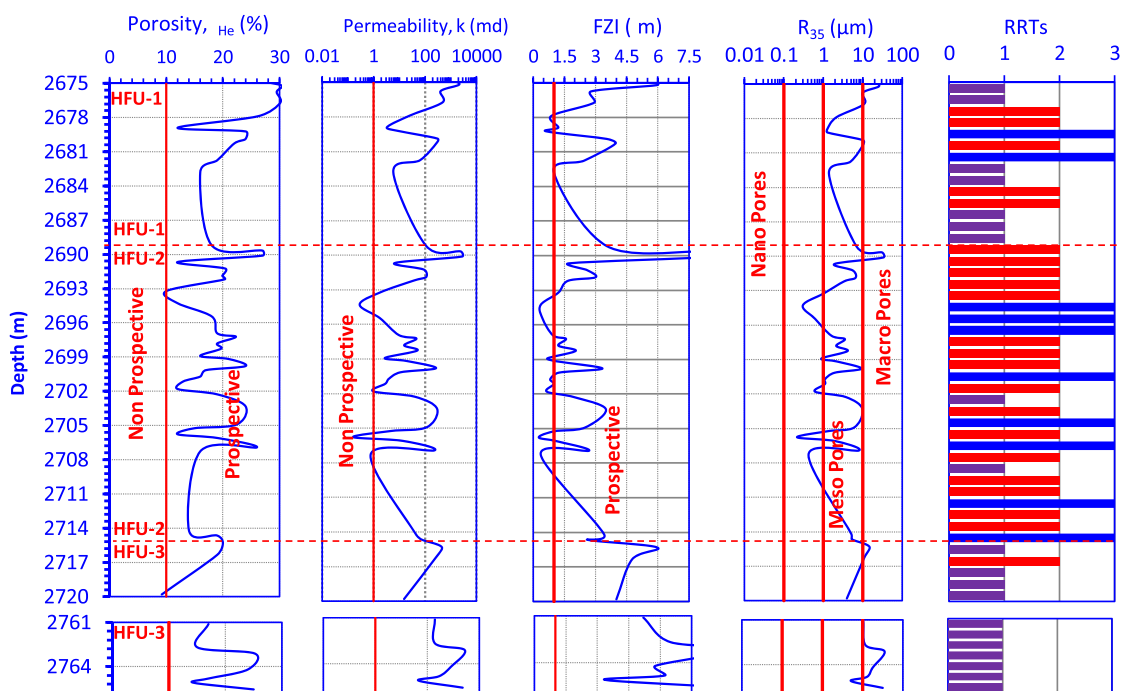


Fig. 19 Vertical presentation of the petrophysical data derived from the core data and their reservoir rock types (RRTs) for the M (depth interval 2675–2720 feet) and L1 (depth interval 2761–2766 feet) units

shorelines. It can be further applied to the other clastic reservoirs in Iraq, Syria, and Jordan. Subdividing the Albian sequence into five rock units states that future exploration and development plans should be deviated to tracing and following up its *M* and *L1* units. Also, discriminating these two units into three reservoir rock types (RRTs) and studying their reservoir characteristics states that the medium-grained sandstone RRT1 samples are characterized by the best reservoir quality and should be considered during exploration.

The revealed petrophysical properties derived from the well log data indicate the presence of two partially isolated compartments separated by thick shale interbeds. The upper compartment represents the lower parts of the *M* unit, while the lower compartment represents the top parts of the *L1* unit.

Conclusions

- The present study indicates that integrating the core and well log data is a successful workflow procedure for depicting the petrophysical and reservoir quality parameters of the Albian sequence in the SWM Oilfield.
- Based on the delineated data, the Albian sequence was subdivided into five rock units (U1, U2, M, L1, and L2).
- Among these units, the M and L1 units are the most promising zones in this sequence. The litho-saturation plot of the available wells indicates that they are composed of fine to medium-grained sandstone alternated with some shale streaks which increase in abundance upward through the M and the U1 units.
- The studied clastic sequences are composed of clean sand with shale volume values less than 8.4%.
- Plotting the hydrocarbon saturation, shale volume, and porosity values as iso-parametric maps indicates that the porosity (17.2–22.0%), the oil saturation (72.0–93.0%), and the net-pay thickness (32.8–77.4 m) increase to the north and the central parts of the field, while the shale volume decreases in the same directions.
- Based on the core data, the rock samples can be subdivided into three reservoir rock types (RRTs). Based on the *X–Y* plots, the permeability is dependent on the porosity and the effective pore radius (R_{35}). Depicting the reservoir quality index (RQI) of the different RRTs indicates its main dependence on permeability and also on porosity as a subsidiary parameter.
- The medium-grained sandstone of the RRT1 is characterized by the best petrophysical and reservoir values (av. $\phi_{He} = 23.0\%$, av. $k = 1581$ mD, av. FZI = 5.53 μm , av. RQI = 2.304 μm , and macropore spaces, i.e., it is characterized by fair to very good reservoir quality).
- On contrary, the fine-grained sandstone samples of the RRT3 have the lowest petrophysical and reservoir quality (av. $\phi_{He} = 17.1\%$, av. $k = 5.49$ mD, av. FZI = 0.603 μm ,

av. RQI = 0.136 μm , and micro- to mesopore spaces, i.e., it is tight reservoir).

- This integrated study delineated that future exploration and development plans in the study area should be applied to the central and northern parts to explore the extension of M unit and upper parts of the L1 unit.

Acknowledgements The authors would like to thank the Editor-in-Chief Prof. Dr. Ali Ghalambor, the associate editor Prof Dr. Abd El-Aziz Khairy Abd El-Aal, and the anonymous reviewers for their valuable comments that highly improved the manuscript quality in its present version.

Funding Open access funding provided by The Science, Technology & Innovation Funding Authority (STDF) in cooperation with The Egyptian Knowledge Bank (EKB).

Declarations

Conflict of interest The authors confirm that they do not have a financial or personal relationship with any party who is interested in this study or could be positively or negatively influenced by the article's content.

Open Access This article is licensed under a Creative Commons Attribution 4.0 International License, which permits use, sharing, adaptation, distribution and reproduction in any medium or format, as long as you give appropriate credit to the original author(s) and the source, provide a link to the Creative Commons licence, and indicate if changes were made. The images or other third party material in this article are included in the article's Creative Commons licence, unless indicated otherwise in a credit line to the material. If material is not included in the article's Creative Commons licence and your intended use is not permitted by statutory regulation or exceeds the permitted use, you will need to obtain permission directly from the copyright holder. To view a copy of this licence, visit <http://creativecommons.org/licenses/by/4.0/>.

References

- Abdeen MM, Ramadan FS, Nabawy BS, El Saadawy O (2021) Sub-surface structural setting and hydrocarbon potentiality of the Komombo and Nuqra Basins, South Egypt: a seismic and petrophysical integrated study. *Nat Resour Res* 30:3575–3603
- Abdelmaksoud A, Radwan AA (2022) Integrating 3D seismic interpretation, well log analysis and static modelling for characterizing the Late Miocene reservoir, Ngatoro area, New Zealand. *Geomech Geophys Geo-Energy Geo-Resources* 8:63. <https://doi.org/10.1007/s40948-022-00364-8>
- Abdelwahhab MA, Radwan AA, Mahmoud H, Mansour A (2022) Geophysical 3Dstatic reservoir and basin modeling of a Jurassic estuarine system (JG-Oilfield, Abu Gharadig basin, Egypt). *J Asian Earth Sci* 225:105067. <https://doi.org/10.1016/j.jseaes.2021.105067>
- Abuamarah BA, Nabawy BS (2021) A proposed classification for the reservoir quality assessment of hydrocarbon-bearing sandstone and carbonate reservoirs: a correlative study based on different assessment petrophysical procedures. *J Natural Gas Sci Eng* 88:103807

- Abuamarah BA, Nabawy BS, Shehata AM, Kassem OMK, Ghrefat H (2019) Integrated geological and petrophysical characterization of oligocene deep marine unconventional poor to tight sandstone gas reservoir. *Mar Pet Geol* 109:868–885
- Abuhagaza AA, El Sawy MZ, Nabawy BS (2021) Integrated petrophysical and petrographical studies for characterization of reservoirs: a case study of Muglad Basin, North Sudan. *Environ Earth Sci* 80:171. <https://doi.org/10.1007/s12665-021-09489-7>
- Al-Ameri TK, Al-Khafaji AJ, Zumberge J (2009) Petroleum system analysis of the Mishrif reservoir in the Ratawi, Zubair, North and South Rumaila oil fields, southern Iraq. *GeoArabia* 14(4):91–108
- Al-Ameri TK, Al-Najar TK, Batten DJ (2001) Palynostratigraphy and palynofacies indications of depositional environments and source potential for hydrocarbons: the mid Cretaceous Nahr Umr and lower Maaddud formations. *Iraq Cretaceous Res* 22(6):735–742
- Alhakeem NSh, Nasser ME, Al-Sharaa GhH (2019) 3D Geological modeling for Yamama Reservoir in Subba, Luhias and Ratawi Oilfields, South of Iraq. *Iraqi J Sci* 60(5):1023–1036
- Al-Khafaji AJ (2015) The Mishrif, Yamama, and Nahr Umr reservoirs petroleum system analysis, Nasiriyah oilfield, Southern Iraq. *Arab J Geosci* 8:781–798
- Alsharhan AS (1991) Sedimentological interpretation of the Albian Nahr Umr formation in the United Arab Emirates. *Sed Geol* 73(3–4):317–327
- Amaefule JO, Altunbay M, Tiab D, Kersey DG, Keelan DK (1993) Enhanced reservoir description: Using core and log data to identify hydraulic (flow) units and predict permeability in uncured intervals/wells. In: The 68th annual technical conference and exhibition of the society of petroleum engineers, Houston, Texas, 3–6 October 1993, SPE-26436-MS 205–220.
- Archie GE (1942) The electrical resistivity log as an aid in determining some reservoir characteristics. *Trans AIME* 146(1):54–62
- Arfania R, Shahriari S (2009) Role of southeastern Sanandaj-Sirjan Zone in the tectonic evolution of Zagros Orogenic Belt. *Iran Island Arc* 18(4):555–576. <https://doi.org/10.1111/j.1440-1738.2009.00680.x>
- Asquith G, Gibson C (1982) Basic well log analysis for geologists. The American Association of Petroleum Geologists. AAPG Methods in Exploration Series, No. 16.
- Asquith G, Krygowski D (2004) Basic well log analysis. AAPG Methods in Exploration Series 16:2004
- Asquith G (1982) Basic well log analysis for geologists. American Association of Petroleum Geologists, Tulsa.
- Audley-Charles MG, Ballantyne PD, Hall R (1988) Mesozoic-Cenozoic rift-drift sequence of Asian fragments from Gondwanaland. *Tectonophysics* 155:317–530
- Baouche R, Nabawy BS (2021) Permeability prediction in argillaceous sandstone reservoirs using fuzzy logic analysis: a case study of triassic sequences, Southern Hassi R'Mel Gas Field. *Algeria J Afr Earth Sci* 173:104049
- Bellen RC, Dunnington HV, Wetzel R, Morton D (1959) Lexique Stratigraphique International Asie. *Iraq* 3C(10a):333
- Buday T, Jassim SZ (1984) Tectonic map of Iraq, scale 1: 1000 000. GEOSURV, Baghdad Iraq.
- Buday T, Jassim SZ (1987) The regional geology of Iraq. v. 2. Tectonism, magmatism and metamorphism. In: MJ Abbas and II Kassab (Eds.) GEOSURV, Baghdad, 352pp.
- Buday T (1980) The regional geology of Iraq, Vol.1, Stratigraphy and Paleogeography. GEOSURV, Baghdad, Iraq, 445p.
- Canard M (2011) Al-Djazira, Djazirat Akhur or Iqlim Akhur. In: Bearman P, Bianquis Th, Bosworth CE, Van Donzel E, Heinrichs WP (eds) Encyclopaedia of Islam, 2nd edn. Leiden: Brill Online, OCLC 624382576.
- David C, Bertauld D, Dautriat J, Sarout J, Menéndez B, Nabawy B (2015) Detection of moving capillary front in porous rocks using X-ray and ultrasonic methods. *Front Phys* 3:53. <https://doi.org/10.3389/fphy.2015.00053>
- El Sharawy MS, Nabawy BS (2018) The role of gamma-ray logs in deciphering geochemical and geological aspects of the Rudeis formation, Gulf of Suez, Egypt. *Arab J Geosci* 11:242. <https://doi.org/10.1007/s12517-018-3560-0>
- El Sawy MZ, Abuhagaza AA, Lashin NBS (2020) Rock typing and hydraulic flow units as a successful tool for reservoir characterization of Bentiu-Abu Gabra sequence, Muglad basin, southwest Sudan. *J Afr Earth Sci* 171:103961
- Elgendy NTH, Abuamarah BA, Nabawy BS, Ghrefat H, Kassem OMK (2020) Pore fabric anisotropy of the Cambrian-Ordovician Nubia sandstone in the Onshore Gulf of Suez, Egypt: a surface outcrop analog. *Nat Resour Res* 29(2):1307–1328
- Ezz El-Din S, Mesbah MA, Kassab MA, Mohamed IF, Cheadle BA, Teama MA (2013) Assessment of petrophysical parameters of clastics using well logs: The Upper Miocene in El-Wastani gas field, onshore Nile Delta, Egypt. *Petrol Explor Dev* 40(4):488–494
- Fallah-Bagdash R, Adab MH, Nabawy BS, Omidpour A, Sadeghi A (2022) Integrated petrophysical and microfacies analyses for a reservoir quality assessment of the Asmari Dolostone sequence in the Khesht Field, SW Iran. *J Asian Earth Sci* 223:104989. <https://doi.org/10.1016/j.jseae.2021.104989>
- Foster BR, Foster PK (2009) Civilizations of Ancient Iraq. Princeton University Press, Princeton. ISBN 978-0-691-13722-3
- Fouad SFA (2010) Tectonic and structural evolution of the Mesopotamia Foredeep, Iraq. *Iraqi Bull Geol Mining* 6(2):41–53
- Handhal AM, Hussein AA (2020) Evaluating the reservoir properties of Nahr Umr Formation at Luhais oil field, southern Iraq using well logs data. *Basrah J Sci* 38(2):294–327
- Handhal AM, Al-Atabi ANSh, Majeed FW (2019) Computation of cementation factor and saturation exponent for selected oil fields in southern Iraq. *J Petrol Res Stud (JPR&S)* 20:113–131
- Haque AKME, Qadri SMT, Bhuiyan MAH, Navid M, Nabawy BS, Hakimi MH, Abd-El-Aal AK (2022) Integrated wireline log and seismic attribute analysis for the reservoir evaluation: a case study of the Mount Messenger Formation in Kaimiro Field, Taranaki Basin, New Zealand. *J Natural Gas Sci Eng* 99:104452. <https://doi.org/10.1016/j.jngse.2022.104452>
- Heslop K, Heslop A (2003) Interpretation of shaly-sands. http://www.lps.org.uk/docs/heslop_shaly_sands.pdf.
- Jassim SZ, Goff JC (2006) Geology of Iraq. Dolin and Moravian Museum, Prague, 341p.
- Jassim SZ, Karim SA, Basri M, Al-Mubarak MA, Munir J (1984) Final report on the regional geological survey of Iraq, v 3, Stratigraphy, GEOSURV, internal report 1447.
- JOGEMEC (2010) Geological study for Ratawi oil field (Ministry of oil Iraq), p 5.
- Kassem AA, Osman O, Nabawy B, Baghdady A, Shehata AA (2022) Microfacies analysis and reservoir discrimination of channelized carbonate platform systems: an example from the Turonian Wata Formation, Gulf of Suez, Egypt. *J Petrol Sci Eng* 212:110272
- Khudhair MH, Al-Zaidy AA (2018) Petrophysical properties and reservoir development of Albian succession in Nasiriyah oil field, southern Iraq. *Iraqi Bull Geol Mining* 14(2):61–69
- Lai J, Wang S, Wang G, Shi Y, Zhao T, Pang X, Fan X, Qin Z, Fan X (2019) Pore structure and fractal characteristics of Ordovician Majiagou carbonate reservoirs in Ordos basin, China. *AAPG Bull* 103(11):2573–2596
- Lai J, Wang S, Zhang C, Wang G, Song Q, Chen X, Yang K, Yuan C (2020) Spectrum of pore types and networks in the deep Cambrian to Lower Ordovician dolostones in Tarim Basin, China. *Mar Petrol Geol* 112:104081
- Larionov VV (1969) Borehole radiometry: Moscow. Nedra, U.S.S.R.
- Liu Y, Liu Y, Zhang Q, Li C, Feng Y, Wang Y, Xue Y, Ma H (2019) Petrophysical static rock typing for carbonate reservoirs based

- on mercury injection capillary pressure curves using principal component analysis. *J Petrol Sci Eng* 181:106175
- Nabawy BS (2013) Impacts of dolomitization on the petrophysical properties of El-Halal Formation, North Sinai, Egypt. *Arab J Geosci* 6(2):359–373
- Nabawy BS, El Sharawy MS (2018) Reservoir assessment and quality discrimination of Kareem Formation using integrated petrophysical data, Southern Gulf of Suez, Egypt. *Mar Petrol Geol* 93:230–246
- Nabawy BS, Shehata AM (2015) Integrated petrophysical and geological characterization for the Sidi Salem-Wakar sandstones, offshore Nile Delta, Egypt. *J Afr Earth Sci* 110:160–175
- Nabawy BS, Sediek KN, Nafee SA (2015) Pore fabric assignment using electrical conductivity of some Albian-Cenomanian sequences in north Eastern Desert, Egypt. *Arab J Geosci* 8(8):5601–5615
- Nabawy BS, Basal AMK, Sarhan MA, Safa MG (2018a) Reservoir zonation, rock typing and compartmentalization of the Tortonian-Serravallian sequence, Temsah Gas Field, offshore Nile Delta, Egypt. *Mar Petrol Geol* 92:609–631
- Nabawy BS, Rashed MA, Mansour AS, Afify WS (2018b) Petrophysical and microfacies analysis as a tool for reservoir rock typing and modelling: Rudeis Formation, off-shore October Oil Field, Sinai. *Mar Petrol Geol* 97:260–276
- Nabawy BS, Elgendy NTH, Gazia MT (2020a) Mineralogic and diagenetic controls on reservoir quality of Paleozoic Sandstones, Gebel El-Zeit, North Eastern Desert, Egypt. *Natural Resources Res* 29:1215–1238
- Nabawy BS, Khalil HM, Fathy MS, Ali F (2020b) Impacts of microfacies type on reservoir quality and pore fabric anisotropy of the Nubia sandstone in the central Eastern Desert, Egypt. *Geol J* 55(6):4507–4524
- Nabawy BS, Mansour AS, Rashed MA, Afify WSM (2020c) Implementation of sedimentary facies and diagenesis on the reservoir quality of the Aquitanian-Burdigalian Rudeis Formation in the Gulf of Suez, Egypt: a comparative surface and subsurface study. *Geol J* 55(6):4543–4563
- Nabawy BS, Lashin AA, Barakat MKh (2022) Implementation of lithofacies and microfacies types on reservoir quality and heterogeneity of the Late Cretaceous Upper Bahariya Member in the Shurouk Field, Shoushan Basin, North Western Desert, Egypt. *J Asian Earth Sci* 224:105014. <https://doi.org/10.1016/j.jseae.2021.105014>
- Numan NMS (2000) Major Cretaceous tectonic events in Iraq. *Raf J Sci* 11(3):32–52
- Owen RM, Nasr SN (1958) The stratigraphy of Kuwait—Basra area. In: Weeks LG (ed) *Habitat of oil*, a symposium, AAPG, pp 1252–1278.
- Powell CMcA, Roots SR, Veevers JJ (1988) Pre-breakup continental extension in East Gondwanaland and early opening of the eastern Indian Ocean. *Tectonophysics* 155:261–283
- Qaradaghi AIF, Abdul-Kareem BM, Al-Jassim JA (2008) Petrography, diagenesis and depositional environment of Nahr Umr Formation, from selected wells in central Iraq. *Iraqi Bull Geol Mining* 4(1):67–94
- Qaradaghi AIF (2001) *Sedimentological Study of the Maaddud Formation in Selected Boreholes from Several Oilfields, Central Iraq*. Unpublished PhD Thesis, University of Baghdad, 120p.
- Radwan AA, Nabawy BS (2022) Hydrocarbon prospectivity of the miocene-pliocene clastic reservoirs, Northern Taranaki basin. New Zealand: Integration of Petrographic and Geophysical Studies. *J Petrol Exploration Prod Technol*. <https://doi.org/10.1007/s13202-021-01451-4>
- Radwan AA, Nabawy BS, Abdelmaksoud A, Lashin A (2021) Integrated sedimentological and petrophysical characterization for clastic reservoirs: a case study from New Zealand. *J Natural Gas Sci Eng* 88:103797
- Radwan AA, Abdelwahhab MA, Nabawy BS, Mahfouz KH, Ahmed MS (2022a) Facies analysis-constrained geophysical 3D-static reservoir modeling of Cenomanian units in the Aghar Oilfield (Western Desert, Egypt): insights into paleoenvironment and petroleum geology of fluviomarine systems. *Mar Pet Geol* 136:105436. <https://doi.org/10.1016/j.marpetgeo.2021.105436>
- Radwan AA, Nabawy BS, Shihata M, Leila M (2022b) Seismic interpretation, reservoir characterization, gas origin and entrapment of the Miocene-Pliocene Mangaa C sandstone, Karewa Gas Field, North Taranaki Basin, New Zealand. *Mar Petrol Geol* 135:105420. <https://doi.org/10.1016/j.marpetgeo.2021.105420>
- Sadooni FN (1997) Stratigraphy and petroleum prospects of Upper Jurassic carbonates in Iraq. *Pet Geosci* 3:233–243
- Sadooni FN (1993) Stratigraphic sequence, microfacies, and petroleum prospect of the Yamama Formation, Lower Cretaceous, southern Iraq. *The American Association of Petroleum Geologists*, 1971–1988.
- Safa MG, Nabawy BS, Basal AMK, Omran MA, Lashin A (2021) A petrographical and petrophysical workflow protocol for studying Implementation of Heterogeneity on Rock Typing and Reservoir Quality of Reefal Limestone: a case study of the Nullipore Carbonates in the Gulf of Suez. *Acta Geol Sinica-Engl Edition* 95(5):1746–1762. <https://doi.org/10.1111/1755-6724.14700>
- Schlumberger (1984) Well evaluation conference; Cairo, Egypt, pp 1–64.
- Schlumberger (1991) *Log interpretation principles/applications*. Schlumberger Educational Services, New York
- Schlumberger (1995) *Well evaluation conference of Egypt*. Technical Editing Services, Chester, 87p.
- Shehata AA, Osman OA, Nabawy BS (2021) Neural network application to petrophysical and lithofacies analysis based on multi-scale data: an integrated study using conventional well log, core and borehole image data. *J Natural Gas Sci Eng* 93:104015
- Shehata, A.A., Sarhan, M.A., 2022. Seismic interpretation and hydrocarbon assessment of the post-rift Cenomanian Bahariya reservoir, Beni Suef Basin, Egypt. *Journal of Petroleum Exploration and Production Technology*. <https://doi.org/10.1007/s13202-022-01520-2>
- Shenawi SH, White JP, Elrafie EA, Kilany KA (2007) Permeability and water saturation distribution by lithologic facies and hydraulic units: a reservoir simulation case study: Society of Petroleum Engineers, SPE-105273-MS.
- Simandoux P (1963) Dielectric measurements in porous media and application to Shaly Formation, *Revue del'Institut Francais du Petrole*, Supplementary Issue 193–215.
- Sissakian VK, Al-Ansari N, Adamo N, Abdullah M, Laue J (2020) Stratigraphy of the Mesopotamian Plain: a critical review. *J Earth Sci Geotech Eng* 10(4):27–56
- Teama MA, Nabawy BS (2016) Petrophysical evaluation of the hydrocarbon potential of the Lower Cretaceous Kharita clastics, North Qarun oil field, Western Desert., Egypt. *J Afr Earth Sci* 121:62–71
- Wilkinson TJ (2000) Regional approaches to mesopotamian archaeology: the contribution of archaeological surveys. *J Archaeol Res* 8(3):219–267. <https://doi.org/10.1023/A:1009487620969,ISSN1573-7756>
- Winland HD (1972) Oil Accumulation in response to pore size changes, Weyburn Field, Saskatchewan. Amoco Production Research Report No. F72-G-25.

Publisher's Note Springer Nature remains neutral with regard to jurisdictional claims in published maps and institutional affiliations.